HHS Public Access

Author manuscript

Cell. Author manuscript; available in PMC 2020 June 13.

Published in final edited form as:

Cell. 2019 June 13; 177(7): 1781–1796.e25. doi:10.1016/j.cell.2019.04.028.

Identification of a DNA N6-adenine methyltransferase complex and its impact on chromatin organization

Leslie Y. Beh[1,2,3], **Galia T. Debelouchina**[2], **Derek M. Clay**[1], **Robert E. Thompson**[2], **Kelsi A. Lindblad**[1], **Elizabeth R. Hutton**[1], **John R. Bracht**[4], **Robert P. Sebra**[5], **Tom W. Muir**[2,*], and **Laura F. Landweber**[1,6,*]

[1]Departments of Biochemistry & Molecular Biophysics and Biological Sciences, Columbia University, New York, NY 10032, USA

[2]Department of Chemistry, Princeton University, Princeton, NJ 08544, USA

[3]Department of Ecology and Evolutionary Biology, Princeton University, Princeton, NJ 08544, USA

[4]Department of Biology, American University, Washington, DC 20016, USA

[5]Icahn Institute and Department of Genetics and Genomic Sciences, Icahn School of Medicine at Mount Sinai, New York, NY 10029, USA

[6]Lead contact

Summary

DNA N6-adenine methylation (6mA) has recently been described in diverse eukaryotes, spanning unicellular organisms to metazoa. Here, we report a DNA 6mA methyltransferase complex in ciliates, termed MTA1c. It consists of two MT-A70 proteins and two homeobox-like DNA-binding proteins, and specifically methylates dsDNA. Disruption of the catalytic subunit, MTA1, in the ciliate *Oxytricha* leads to genome-wide loss of 6mA and abolishment of the consensus ApT dimethylated motif. Mutants fail to complete the sexual cycle, which normally coincides with peak MTA1 expression. We investigate the impact of 6mA on nucleosome occupancy *in vitro* by reconstructing complete, full-length *Oxytricha* chromosomes harboring 6mA in native or ectopic positions. We show that 6mA directly disfavors nucleosomes *in vitro* in a local, quantitative manner, independent of DNA sequence. Furthermore, the chromatin remodeler ACF can overcome

*Correspondence: muir@princeton.edu (T.W.M.), Laura.Landweber@columbia.edu (L.F.L.).

Author contributions

L.Y.B. conceived the project, synthesized chromosomes, performed computational and experimental analysis for all Figures and Tables, and wrote the manuscript. G.T.D. synthesized chromosomes and prepared *Xenopus* histones. D.M.C. generated MTA1 mutants. R.E.T. synthesized 6mA nucleoside standards for mass spectrometry. K.A.L. processed raw SMRT-seq data. E.R.H. performed 6mA IP-seq. J.R.B. prepared *Oxytricha* DNA for SMRT-seq. R.P.S. performed SMRT-seq. T.W.M. and L.F.L. conceived the project and analyzed data. G.T.D, T.W.M, and L.F.L. edited the manuscript.

Declaration of Interests

The authors declare no competing interests.

this effect. Our study identifies a diverged DNA N6-adenine methyltransferase, and defines the role of 6mA in chromatin organization.

Graphical Abstract

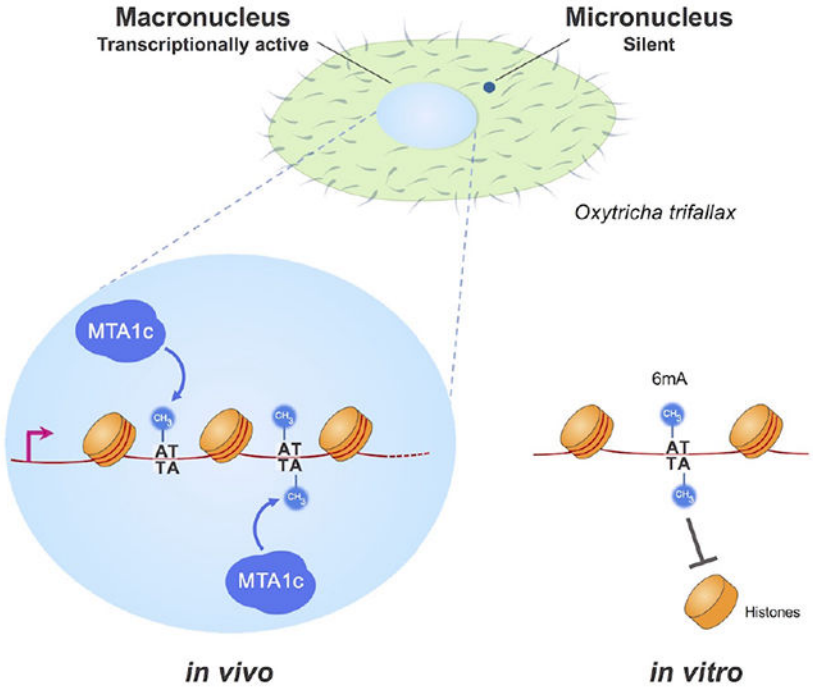

Keywords

DNA methylation; N6-methyladenine; nucleosome positioning; synthetic chromosomes; chromatin remodeling

Introduction

Covalent modifications on DNA have long been recognized as a hallmark of epigenetic regulation. DNA N6-methyladenine (6mA) has recently come under scrutiny in eukaryotic systems, with proposed roles in retrotransposon or gene regulation, transgenerational epigenetic inheritance, and chromatin organization (Luo et al., 2015). 6mA exists at low levels in *Arabidopsis thaliana* (0.006%- 0.138% 6mA / dA), rice (0.2%), *C. elegans* (0.01–0.4%), *Drosophila* (0.001-0.07%), *Xenopus laevis* (0.00009%), mouse ES cells (0.0006 – 0.007%), human cells (Greer et al., 2015; Koziol et al., 2015; Liang et al., 2018; Wu et al., 2016; Xiao et al., 2018; Zhang et al., 2015; Zhou et al., 2018) and the mouse brain (Yao et al., 2017), although it accumulates in abundance (0.1–0.2%) during vertebrate embryogenesis (Liu et al., 2016). Disruption of DMAD, a 6mA demethylase, in the *Drosophila* brain leads to the accumulation of 6mA and Polycomb-mediated silencing (Yao et al., 2018). The existence of 6mA in mammals remains a subject of debate. Quantitative LC-MS analysis of HeLa and mouse ES cells failed to detect 6mA above background levels (Schiffers et al., 2017). A recent study, however, reported that loss of 6mA in human cells

promotes tumor formation (Xiao et al., 2018), suggesting that 6mA is a biologically relevant epigenetic mark.

In contrast to metazoa, 6mA is abundant in various unicellular eukaryotes, including ciliates (0.18 – 2.5%) (Ammermann et al., 1981; Cummings et al., 1974; Gorovsky et al., 1973; Rae and Spear, 1978), and the green algae *Chlamydomonas* (0.3 – 0.5%) (Fu et al., 2015; Hattman et al., 1978). High levels of 6mA (up to 2.8%) were also recently reported in basal fungi (Mondo et al., 2017). Ciliates have long served as powerful models for the study of chromatin modifications (Brownell et al., 1996; Liu et al., 2007; Strahl et al., 1999; Taverna et al., 2002; Wei et al., 1998). They possess two structurally and functionally distinct nuclei within each cell (Bracht et al., 2013; Yerlici and Landweber, 2014). In the ciliate *Oxytricha trifallax*, the germline *micronucleus* is transcriptionally silent and contains ~100 megabase-sized chromosomes (Chen et al., 2014). In contrast, the somatic *macronucleus* is transcriptionally active, being the sole locus of Pol II-dependent RNA production in non-developing cells (Khurana et al., 2014). The *Oxytricha* macronuclear genome is extraordinarily fragmented, consisting of ~16,000 unique chromosomes with a mean length of ~3.2kb, most encoding a single gene. Macronuclear chromatin yields a characteristic ~200bp ladder upon digestion with micrococcal nuclease, indicative of regularly spaced nucleosomes (Gottschling and Cech, 1984; Lawn et al., 1978; Wada and Spear, 1980). Yet it remains unknown how and where nucleosomes are organized within these miniature chromosomes, and if this in turn regulates (or is regulated by) 6mA deposition.

Intriguingly, in green algae, basal yeast, and ciliates, 6mA is enriched in ApT dinucleotide motifs within nucleosome linker regions near promoters (Fu et al., 2015; Hattman et al., 1978; Karrer and VanNuland, 1999; Mondo et al., 2017; Pratt and Hattman, 1981; Wang et al., 2017). Here we identify four ciliate proteins – named MTA1, MTA9, p1, and p2 – necessary for 6mA methylation. MTA1 and MTA9 contain divergent MT-A70 domains, while p1 and p2 are homeobox-like proteins that likely function in DNA binding. We delineate key biochemical properties of this methyltransferase and dissect the function of 6mA *in vitro* and *in vivo*.

Results

Epigenomic profiles of chromatin and transcription in *Oxytricha*

We generated genome-wide *in vivo* maps of nucleosome positioning, transcription, and 6mA in the macronuclei of asexually growing (vegetative) *Oxytricha trifallax* cells using MNase-seq, poly(A)+ RNA-seq, TSS-seq, and single molecule real time (SMRT) sequencing (Figure 1). The smallest *Oxytricha* chromosome is only 430bp in length, with a single well-positioned nucleosome. Strikingly, 6mA is enriched in three consecutive nucleosome depleted regions directly downstream of transcription start sites (TSSs; Figure 1A). Each region contains varying levels of 6mA (Figure 1B), with the +1/+2 nucleosome linker being most densely methylated (Table S1). In general, highly transcribed chromosomes tend to bear more 6mA, suggesting a positive role of this DNA modification in gene regulation (Figure 1C). The majority of methylation marks are located within an ApT motif (Figures 1D and 1E). 6mA occurs on sense and antisense strands with approximately equal frequency, indicating that the underlying methylation machinery does not function strand-

specifically. Quantitative LC-MS analysis confirmed the presence of 6mA in *Oxytricha* (Figure S1; see Methods).

Purification and reconstitution of the ciliate 6mA methyltransferase, MTA1c

To uncover the functions of 6mA *in vivo*, we set out to identify and disrupt putative 6mA methytransferases (MTases). The *Oxytricha* genome encodes a large number of candidate methyltransferases (Table S2), rendering it impractical to test gene function, one at a time or in combination. To identify the ciliate 6mA MTase, we undertook a biochemical approach by fractionating nuclear extracts and identifying candidate proteins that co-purified with DNA methylase activity. The organism of choice for this experiment was *Tetrahymena thermophila*, a ciliate that divides significantly faster than *Oxytricha* (~2 hours vs 18 hours); (Cassidy-Hanley, 2012; Laughlin et al., 1983). This faster growth time rendered it feasible to culture large amounts of *Tetrahymena* cells for nuclear extract preparation. *Tetrahymena* and *Oxytricha* exhibit similar genomic localization and 6mA abundance (Figures S1 and S2A–F). We thus reasoned that the enzymatic machinery responsible for 6mA deposition is conserved between *Tetrahymena* and *Oxytricha*, and that *Tetrahymena* could serve as a tractable biochemical system for identifying the ciliate 6mA MTase.

We prepared nuclear extracts from log-phase *Tetrahymena* cells, since 6mA could be readily detected at this developmental stage through quantitative mass spectrometry and PacBio sequencing (Figures S1 and S2A–F). Nuclear extracts were incubated with radiolabeled S-adenosyl-L-methionine and PCR-amplified DNA substrate to assay for DNA methylase activity. Passage of the nuclear extract through an anion exchange column resulted in the elution of two distinct peaks of DNA methylase activity, both of which were heat sensitive (Figure 2C, S3A, S3B). Western blot analysis confirmed that both peaks of activity mediate methylation on 6mA (Figure S3C). The resulting fractions were further purified and subjected to mass spectrometry. Only four proteins – termed MTA1, MTA9, p1 and p2 – were detected at higher abundance in fractions with high DNA methylase activity (Figures 2C and 2D). p1 and p2 contain homeobox-like domains, suggesting a DNA binding function for an undetermined process (Figure S3D). On the other hand, MTA1 and MTA9 are both MT-A70 proteins. Such domains are widely known to mediate m^6A RNA methylation in eukaryotes (Liu et al., 2014). MTA1 and MTA9 received the large majority of peptide matches, relative to all other MT-A70 genes encoded by the *Tetrahymena* genome (Figure 2D and Table S3). Curiously, although poly(A)-selected RNA transcripts were present from all MT-A70 genes (Figure 2D), almost all peptides in fractions with high DNA methylase activity corresponded to MTA1 and MTA9. The poly(A)+ RNA expression profiles of MTA1, MTA9, p1, and p2 are remarkably similar (Figure S2K), peaking early in the sexual cycle. This coincides with a sharp increase in nuclear 6mA, as evidenced from immunostaining (Wang et al., 2017). Accumulation of MTA1, MTA9, p1, and p2 therefore correlates with the presence of 6mA *in vivo*.

We next investigated the phylogenetic relationship of MTA1 and MTA9 to other eukaryotic MT-A70 domain-containing proteins. Two widely studied mammalian MT-A70 proteins – METTL3 and METTL14 (Ime4 and Kar4 in yeast) – form a heterodimeric complex that is responsible for m^6A methylation on mRNA. METTL3 is the catalytically active subunit,

while METTL14 functions as an RNA-binding scaffold protein (Śledź and Jinek, 2016; Wang et al., 2016a, 2016b). MTA1 and MTA9 derive from distinct monophyletic clades, outside of those that contain mammalian METTL3, METTL14, and *C. elegans* DAMT-1 (METTL4) (Figure 2A). Thus, MTA1 and MTA9 are divergent MT-A70 family members that are phylogenetically distinct from all previously studied RNA and DNA N6-methyladenine MTases. We then asked whether MTA1 and MTA9 are also present in other eukaryotes with a similar occurrence of 6mA in ApT motifs as *Tetrahymena*. We queried the genomes of *Oxytricha*, green algae, and eight basal yeast species, all of which exhibit this distinct methylation pattern (as evidenced from Figure 1, Figure S2A–E, (Fu et al., 2015), and (Mondo et al., 2017)). For all of these taxa, we can identify MT-A70 homologs that are monophyletic with MTA1 and MTA9 (Figure 2B). On the other hand, MT-A70 homologs from multicellular eukaryotes, including *Arabidopsis*, *C. elegans*, *Drosophila*, and mammals, grouped exclusively with METTL3, METTL14, and METTL4 lineages, but not MTA1 or MTA9. None of these latter genomes exhibit a consensus ApT dinucleotide methylation motif for 6mA (Greer et al., 2015; Koziol et al., 2015; Liang et al., 2018; Liu et al., 2016; Wu et al., 2016; Xiao et al., 2018; Zhang et al., 2015). We note that the absence of an ApT dinucleotide motif is based on data from a limited number of cell types, developmental stages, and culture conditions tested in these studies. Nonetheless, within the scope of currently available data, the presence of MTA1 and MTA9 correlates with the distinctive genomic localization of 6mA within ApT motifs.

We then sought to determine whether MTA1 and/or MTA9 are *bona fide* 6mA methyltransferases. MTA1, but not MTA9, contains a catalytic DPPW motif (Figure S3E)—a hallmark of N6-adenosine methyltransferases (Iyer et al., 2016). Surprisingly, recombinant full length *Tetrahymena* MTA1 and MTA9 (Figure S3G) showed no detectable DNA methyltransferase activity, individually or together (Figure 2E). Examination of the MTA1 and MTA9 sequences revealed that neither protein possesses a predicted nucleic acid binding domain (Figure S3D). In contrast, METTL3, which catalyzes m^6A methylation on RNA, contains two tandem CCCH-type zinc finger motifs, necessary for RNA binding (Huang et al., 2018; Wang et al., 2016a). Additional co-factors may thus be necessary for MTA1/7 to engage DNA substrates. Indeed, the p1 and p2 proteins that co-elute with MTA1/7 in nuclear extracts possess homeobox-like domains predicted to bind DNA. We then tested whether these accessory factors, in addition to MTA1/7, are necessary for 6mA methylation. Strikingly, mixing recombinant, full length p1, p2, MTA1, and MTA9 resulted in robust 6mA methylation *in vitro* (Fig 2E and 2F). This activity was abolished when each protein was omitted, indicated that all four are necessary for 6mA methylation. Furthermore, MTA1 harboring a D209A mutation in the catalytic DPPW motif showed no activity, even in the presence of MTA9, p1 and p2 (Figure 2E). We also created double mutations in MTA1 (N370A, E371A), which lie in the conserved region that interacts with the 2’ and 3’-hydroxyl groups of the ribose moiety in the SAM cofactor (Figure 2E). This mutant protein also exhibited no 6mA methylase activity. Taken together, we find that four proteins – MTA1, MTA9, p1, and p2 – are necessary for 6mA methylation *in vitro*, with MTA1 the likely catalytic subunit. Henceforth, we refer to these four proteins as the putative MTA1 complex (MTA1c).

Purification of the MTA1c proteins from an *E. coli* over-expression system raises the possibility of methyltransferase activity arising from contaminating *Dam* methylase; however, we exclude this possibility for three reasons: 1) the DNA substrate used in this assay does not contain 5'-NATC-3' sites, which are recognized and methylated by *Dam* methylase (Horton et al., 2006). 2) Methyltransferase activity was only observed when all four recombinant proteins were incubated with DNA. If contaminating *Dam* methylase were present in one or more of these protein preparations, then background activity should be observed when subsets of these proteins are used in the assay. 3) Mutation of MTA1 catalytic residues leads to loss of methylation, which is also inconsistent with contaminating methyltransferase activity.

MTA1c preferentially methylates ApT dinucleotides in dsDNA

We next investigated the substrate preferences of MTA1c. First, *in vitro* transcription was performed to generate dsRNA and ssRNA from the input dsDNA substrate. We found that MTA1c methylates dsDNA but not dsRNA or ssRNA of the same sequence, indicating that it is selective for DNA over RNA (Figure S3H). We then generated a series of dsDNA substrates by annealing oligonucleotide pairs of different length and sequence. All of these substrates are *bona fide Tetrahymena* genomic DNA sequences. In each case, MTA1c can methylate the annealed dsDNA but not ssDNA (Figures 2G and S3I).

Since 6mA methylation mainly lies in ApT dinucleotides *in vivo* (Figures 1D and S2D), we asked whether MTA1c preferentially methylates this motif. To test this, we used a 27 bp dsDNA substrate with two ApT dinucleotides in its native sequence (Figure 2G). We disrupted one or both ApT motifs (Figure 2G) by mutually swapping the 5' A with a neighboring base 5'-C**A**T-3' → 5'-**A**C**T**-3'. Disrupting both ApT dinucleotides resulted in >10-fold reduced methylation, while disrupting only one motif led to a 2–4 fold loss (Figures 2G and S3K).

Given that 6mA occurs on both strands of genomic DNA *in vivo* (Figure 1E and S2E), we asked whether pre-existing methylation of one strand affects MTA1c activity. DNA oligonucleotides were nonspecifically methylated with 6mA using *EcoGII* (Murray et al., 2018), a bacterial 6mA methyltransferase. After rigorous purification, samples were annealed to an unmethylated, complementary strand to yield hemimethylated dsDNA (Figure S3F). MTA1c activity was 3–3.5 fold higher on hemimethylated substrates, relative to unmethylated dsDNA (Figure 2G). This effect was similar between dsDNA substrates pre-methylated on the sense or antisense strand, consistent with the lack of an overt strand bias in 6mA locations *in vivo* (Figure 1E and S2E). Importantly, the increase in MTA1c activity cannot be attributed to contaminating *EcoGII* in hemimethylated substrates, since no activity was observed in the absence of MTA1c (Figure S3J). Thus, pre-existing 6mA methylation stimulates MTA1c, indicative of a positive feedback loop.

We then asked whether MTA1c activity is modulated not only by the dinucleotide motif sequence *per se*, but also by flanking sequences. This may manifest as the wide variation in frequency of DNA 4-mers containing a methylated ApT dinucleotide 5'-NA*TN-3' *in vivo* (Figure S3M). To test this, we used a dsDNA substrate containing two ApT dinucleotides, both within a 5'-C**AT**T-3'. Swapping of the ApT motif with the adjacent downstream DNA

residue produced substrates containing 5’-T**AT**A-3’ (Figure S3L). Substrates with this change at both locations had 4-fold less MTA1c activity, and an intermediate effect when only one dinucleotide was altered (Figures S3L). These data indicate that 5’-C**AT**T-3’ is the preferred methylation substrate, consistent with the higher frequency of methylated 5’-C**A*T**T-3’ versus 5’-T**A*T**A-3’ in both *Tetrahymena* and *Oxytricha* genomic DNA (Figure S3M). The difference in frequency of methylated sequences cannot simply be attributed to the higher frequency of the 4nt 5’-C**AT**T-3’ motif vs. 5’-T**AT**A-3’ in the genome, because the opposite trend is observed (Figure S3N). Thus, MTA1c is sensitive to variation in DNA sequences flanking the ApT dinucleotide motif.

MTA1 is necessary for 6mA methylation *in vivo*

Having established that MTA1c is a 6mA methyltransferase, we tested the role of MTA1c in mediating 6mA methylation *in vivo* in *Oxytricha*, for which we have ease of generating mutants. The genome-wide localization of 6mA is conserved between *Oxytricha* and *Tetrahymena* (Figures 1 and S2A–F), implying similar underlying enzymatic machinery. Indeed, all four component genes – MTA1, MTA9, p1, and p2 – are clearly conserved between both species (Figure S2G–J). The DPPW catalytic motif is also completely conserved in *Tetrahymena* and *Oxytricha* MTA1 but not MTA9, suggesting that MTA1 is the likely catalytic subunit of MTA1c in both ciliates (Figure S3E). To abrogate MTA1c function, we disrupted the *Oxytricha* MTA1 gene by inserting an ectopic DNA sequence 49 bp downstream of the start codon, resulting in a frameshift mutation and loss of the C-terminal MTase domain (Figure 3A). *Oxytricha* has two MTA1 paralogs, named MTA1 and MTA1-B (Figures 2A and S2G). We focused on MTA1 because MTA1-B is not expressed in vegetative *Oxytricha* cells (Swart et al., 2013), which we used to profile 6mA locations via SMRT-seq. Dot blot analysis confirmed a significant reduction in bulk 6mA levels in mutant lines (Figure 3B). We then examined 6mA positions at high resolution using SMRT-seq to understand how the DNA methylation landscape is altered in *mta1* mutants. Notably, these mutants exhibit genome-wide loss of 6mA, with complete abolishment of the dimethylated ApT motif, and reduction in frequency of all other methylated dinucleotide motifs (Figures 3C–E). These findings are consistent across all biological replicates and are robust to wide variation in SMRT-seq parameters for calling 6mA modifications (Figure S4B–D). It cannot be attributed to variation in sequencing coverage between wild type and mutant lines. The loss of methylated ApT dinucleotides in *mta1* mutants is consistent with our *in vitro* data suggesting that MTA1c primarily methylates ApT sites (Figures 2G and S3K). The Inter Pulse Duration ratio (degree of polymerase slowing during PacBio sequencing due to presence of a modified base) and estimated fractional methylation also decreased significantly at called 6mA sites in *mta1* mutants ($p < 2.2 \times 10^{-16}$, Wilcoxon rank-sum test) (Figure S4A). MTA1 is therefore necessary for a significant proportion of *in vivo* 6mA methylation events in *Oxytricha*.

What are the phenotypic consequences of 6mA loss *in vivo*? It has been proposed that DNA methylation – including 6mA and cytosine methylation – is involved in nucleosome organization (Fu et al., 2015; Huff and Zilberman, 2014). We thus asked whether nucleosome organization is altered in *mta1* mutants. We quantified nucleosome “fuzziness”, defined as the standard deviation of MNase-seq read locations surrounding the called

nucleosome peak (Lai and Pugh, 2017; Mavrich et al., 2008). A poorly positioned nucleosome consists of a shallow and wide peak of MNase-seq reads, manifested by a high fuzziness score. Nucleosomes were first grouped according to the change in flanking 6mA between wild type and *mta1* mutant cells (Figure S5A–G). The nucleosomes that experience large changes in flanking 6mA exhibit significantly greater increase in fuzziness, compared to nucleosomes with little change in flanking 6mA (Figure S5A and S5D). Such nucleosomes also exhibit changes in occupancy that are consistent with an increase in fuzziness (Figures S5A and S5E). These results are robust to variation in MNase digestion (Figure S7C–D). On the other hand, nucleosome linkers do not change in length or occupancy, even though 6mA is lost from these regions (Figures S5B,C,F,G). We conclude that 6mA exerts subtle effects on nucleosome organization *in vivo*.

6mA disfavors nucleosome occupancy across the genome *in vitro* but not *in vivo*

Multiple factors, including 6mA, DNA sequence, and chromatin remodeling complexes, may collectively contribute to nucleosome organization *in vivo*. The effect of 6mA could therefore be masked by these elements. We next sought to determine whether 6mA directly impacts nucleosome organization. To this end, we assembled chromatin *in vitro* using *Oxytricha* gDNA, which contains cognate 6mA. To obtain a matched negative control lacking DNA methylation, 98 complete chromosomes were amplified using PCR (Figure 4A), purified and subsequently mixed together in stoichiometric ratios to obtain a “mini-genome” (Figure 4B). These chromosomes collectively reflect overall genome properties, including AT content, chromosome length, and transcriptional activity (Table S4). Native genomic DNA (containing 6mA) and amplified mini-genome DNA (lacking 6mA) were each assembled into chromatin *in vitro* using *Xenopus* or *Oxytricha* histone octamers (Figures S6A–F) and analyzed using MNase-seq. We computed nucleosome occupancy from the native genome and mini-genome samples across 199,795 overlapping DNA windows, spanning all base-pairs in the 98 chromosomes. This allowed the direct comparison of nucleosome occupancy in each window of identical DNA sequence, with and without 6mA (Figures 4C and 4D). Windows exhibit lower nucleosome occupancy with increasing 6mA, confirming the quantitative nature of this effect. Furthermore, similar trends were observed for both native *Oxytricha* and recombinant *Xenopus* histones, suggesting that the effects of 6mA on nucleosome organization arise mainly from intrinsic features of the histone octamer rather than from species-specific variants (Figure 4C and 4D). These results are also robust to the extent of MNase digestion of reconstituted chromatin (Figure S7A).

We then directly compared the impact of 6mA on nucleosome occupancy *in vitro* and *in vivo*. Loss of 6mA *in vitro* is achieved by mini-genome construction, while loss *in vivo* is achieved by the *mta1* mutation. For each overlapping DNA window, we calculated the difference in nucleosome occupancy: 1) between native genome and mini-genome DNA *in vitro*, and 2) between wild type and *mta1* mutants *in vivo* (Figure 4C). Nucleosome occupancy is indeed lower in the presence of 6mA methylation *in vitro* (Figures 4C and 4D). In contrast, no change in nucleosome occupancy is observed *in vivo* (Figures 4C and 4E). This result is consistent with our earlier analysis of linker occupancy in *mta1* mutants (Figure S5C and S5G). We note that highly methylated DNA windows show greater change in 6mA relative to *mta1* mutants (Figure 3D). Yet, these windows do not change in

nucleosome occupancy *in vivo*. We conclude that 6mA methylation locally disfavors nucleosome occupancy *in vitro*, but that this intrinsic effect can be overcome by endogenous chromatin factors *in vivo*.

Modular synthesis of epigenetically defined chromosomes

The above experiments used kinetic signatures from SMRT-seq data to infer the presence of 6mA marks in genomic DNA. We next sought to confirm that 6mA is directly responsible for disfavoring nucleosomes *in vitro*, and to understand how this effect could be overcome by cellular factors. 6mA-containing oligonucleotides were annealed and subsequently ligated with DNA building blocks to form full length chromosomes. Importantly, these chromosomes contain 6mA at all locations identified by SMRT-seq *in vivo*. The representative chromosome, *Contig1781.0*, is 1.3kb, contains a clearly defined TSS, and encodes a single highly transcribed gene with a predicted RING finger domain. The length and gene structure are characteristic of typical *Oxytricha* chromosomes (Figure 5A). We independently validated the location of 6mA *in vivo* by sequencing chromosomal DNA immunoprecipitated with an anti-6mA antibody (Figure 5A).

Four chromosome variants were synthesized, with cognate 6mA sites on neither, one, or both DNA strands (chromosomes 1–4 in Figures 5B–C). Chromatin was assembled by salt dialysis with either *Oxytricha* or *Xenopus* nucleosomes and subsequently digested with MNase to obtain mononucleosomal DNA (Figures 6A and S6G). Tiling qPCR was used to quantify nucleosome occupancy at ~50bp increments along the entire length of the synthetic chromosome (Figure 6B). The fully methylated locus exhibits a ~46% reduction in nucleosome occupancy relative to the unmethylated variant, while hemimethylated chromosomes containing half the number of 6mA marks showed intermediate nucleosome occupancy at the corresponding region (Figure 6B). The reduction in nucleosome occupancy was confined to the methylated region, and not observed across the rest of the chromosome. Similar trends were observed when chromatin was assembled using the NAP1 histone chaperone (Figure S7F, top panel), indicating that this effect is not an artifact of the salt dialysis method. Furthermore, moving 6mA to an ectopic location (chromosome 5 in Figures 5B–C) decreases nucleosome occupancy at that site (Figure 6C). We conclude that 6mA directly disfavors nucleosome occupancy in a local, quantitative manner *in vitro*.

Chromatin remodelers restore nucleosome occupancy over 6mA sites

Nucleosome occupancy *in vivo* is influenced not only by DNA sequences, but also by trans-acting factors such as ATP-dependent chromatin remodeling factors (Struhl and Segal, 2013). We used synthetic, methylated chromosomes to test how the well-studied chromatin remodeler ACF responds to 6mA in native DNA. ACF generates regularly spaced nucleosome arrays *in vitro* and *in vivo* (Clapier and Cairns, 2009; Ito et al., 1997). Its catalytic subunit ISWI is conserved across eukaryotes, including *Oxytricha* and *Tetrahymena* (Table S2). Synthetic chromosomes were assembled into chromatin by salt dialysis as before, then incubated with ACF in the presence of ATP (Figures S6H and 6D). We find that ACF partially – but not completely – restores nucleosome occupancy over the methylated locus in an ATP-dependent manner (Figure 6D). This effect is observed when ACF was added to chromatin assembled by salt dialysis or the NAP1 histone chaperone (Figure 6D

and S7F). ACF also restores nucleosome occupancy over methylated loci in native genomic DNA (Figures 6E and S6I), indicating that the effect is not restricted to a single chromosome. This result is robust to the extent of MNase digestion (Figure S7B). Although the heterologous system used here may differ from endogenous chromatin assembly factors in *Oxytricha*, our experiment illustrates the principle that *trans*-acting factors can counteract or even overcome the effect of 6mA on nucleosome organization.

Disruption of MTA1 impacts gene expression and sexual development

Since *mta1* mutants exhibit genome-wide loss of 6mA, we assayed these cells for transcriptional changes by poly(A)+ RNAseq. Only a small minority of genes show significant changes in gene expression (10% FDR, Figure 7A). To examine the methylation status of these differentially expressed genes, we grouped them according to "starting" methylation level, as defined by the total number of 6mA marks near the TSS in wild type cells. Genes exhibit two distinct transcriptional responses: those with low starting levels of 6mA exhibit a small change in 6mA between wild type and mutant cells (Figure 3D) and tend to be significantly upregulated in mutant lines ($p = 2.8 \times 10^{-9}$, Fisher's exact test; and Figure 7B). Surprisingly, genes with high starting 6mA are not enriched in differentially expressed genes ($p > 0.1$, Fisher's exact test), even though they exhibit greater loss of 6mA in mutants (Figure 3D). Steady state RNAseq levels are therefore largely robust to drastic changes in 6mA levels. Since most, but not all, 6mA is lost from *mta1* mutants (Figure 3C), it is also possible that residual DNA methylation across the genome sufficiently buffers genes from changes in transcription.

Because the aforementioned phenotypic changes were assayed in vegetative *Oxytricha* cells, we asked whether MTA1 may play roles outside of this developmental state. MTA1 transcript levels are markedly upregulated in the sexual cycle, as assayed by poly(A)+ RNAseq (Figure 7C). Strikingly, *mta1* mutants fail to complete the sexual cycle when induced to mate, and display complete lethality (Figure 7D). Our data do not exclude the possibility that m^6A RNA methylation, in addition to 6mA DNA methylation, is also impacted by MTA1 loss during development. Further studies would clarify the role of MTA1 in these pathways.

Discussion

Here, we identify MTA1c as a conserved, hitherto undescribed 6mA methyltransferase. It consists of two MT-A70 proteins (MTA1 / MTA9) and two homeobox-like proteins (p1 / p2). The composition of MTA1c provides immediate insights into how it specifically methylates DNA (Figure 7F). MTA1 likely mediates transfer of the methyl group from SAM to the acceptor adenine moiety, given that it contains conserved amino acid residues implicated in catalysis and SAM binding (Figure S3E). Indeed, we show that these residues are necessary for its activity (Figure 2E). While MTA1 constitutes the catalytic center, it lacks a CCCH-type zinc finger domain that is necessary for RNA binding in the canonical m^6A methyltransferase METTL3. Instead, nucleic acid binding is likely assumed by the homeobox-like domains in p1 and p2, which are known to specifically engage dsDNA through helix-turn-helix motifs.

The observation that MTA1c is more active in the presence of pre-methylated DNA templates is reminiscent of the CpG methyltransferase DNMT1. Yet, MTA1c and DNMT1 exhibit distinct protein domain architectures. Further biochemical studies are required to elucidate the molecular basis of this property. A distinct MT-A70 protein, named TAMT-1, was recently reported to act as a 6mA methyltransferase in *Tetrahymena*, (Luo et al., 2018), suggesting that multiple enzymes mediate 6mA deposition. It remains to be determined how MTA1c and TAMT-1 collectively mediate DNA methylation at various developmental stages, and whether cross-talk occurs between these enzymes.

In addition to identifying the ciliate 6mA methyltransferase, we investigated the function of 6mA *in vitro* by building epigenetically defined chromosomes. We show that 6mA directly disfavors nucleosome occupancy in a local, quantitative manner, independent of DNA sequence (Figure 7E). Our experiments do not reveal exactly how 6mA disfavors nucleosome occupancy. Early studies suggest that 6mA destabilizes dA:dT base pairing, leading to a decrease in the melting temperature of DNA (Engel and von Hippel, 1978). Whether this or some other property of 6mA contributes to lowered nucleosome stability awaits further investigation.

Intriguingly, nucleosome organization exhibits only subtle changes after genome-wide loss of 6mA (Figure 7E). Only a small set of genes (<10%) is transcriptionally dysregulated. It is possible that residual 6mA in *mta1* mutants could mask relevant phenotypes. Nonetheless, our results caution against interpreting 6mA function solely based on correlation with genomic elements. We also find that 6mA intrinsically disfavors nucleosomes *in vitro*, but – crucially – this effect can be overridden by distinct factors *in vitro* and *in vivo*. We propose that phased nucleosome arrays are first established *in vivo*, which then restrict MTAI-mediated methylation to linker regions due to steric hindrance. This in turn decreases the fuzziness of flanking nucleosomes, reinforcing chromatin organization. Therefore, 6mA tunes nucleosome organization *in vivo*. Our data do not support the hypothesis that nucleosome phasing is established by pre-deposited 6mA.

More broadly, our work showcases the utility of *Oxytricha* chromosomes for advancing chromatin biology. By extending current technologies (Müller et al., 2016), it should be feasible to introduce both modified nucleosomes and DNA methylation in a site-specific manner on full-length chromosomes. Such ‘designer’ chromosomes will serve as powerful tools for studying DNA-templated processes such as transcription within a fully native DNA environment.

STAR Methods

Contact for reagent and resource sharing

Further information and requests for resources and reagents should be directed to Laura Landweber (Laura.Landweber@columbia.edu).

Experimental model and subject details

Oxytricha trifallax—Vegetative *Oxytricha trifallax* strain JRB310 was cultured at a density of 1.5×10^7 cells/L to 2.5×10^7 cells/L in Pringsheim media (0.11mM Na_2HPO_4,

0.08mM $MgSO_4$, 0.85mM $Ca(NO_3)_2$, 0.35mM KCl, pH 7.0) and fed daily with *Chlamydomonas reinhardtii*. Cells were filtered through cheesecloth to remove debris and collected on a 10μm Nitex mesh for subsequent experiments.

Tetrahymena thermophila—Stock cultures of vegetative *Tetrahymena thermophila* strain SB210 were maintained in Neff medium (0.25% w/v proteose peptone, 0.25% w/v yeast extract, 0.5% glucose, 33.3μM $FeCl_3$). These cultures were inoculated into SSP medium (2% w/v proteose peptone, 0.1% w/v yeast extract, 0.2% w/v glucose, 33μM $FeCl_3$) and grown to log-phase (~3.5×10^5 cells/mL) through constant shaking at 125 rpm / 30°C.

Method details

***in vivo* MNase-seq—**3×10^5 vegetative *Oxytricha* cells were fixed in 1% w/v formaldehyde for 10 min at room temperature with gentle shaking, and then quenched with 125mM glycine. Cells were lysed by dounce homogenization in lysis buffer (20mM Tris pH 6.8, 3% w/v sucrose, 0.2% v/v Triton X-100, 0.01% w/v spermidine trihydrochloride) and centrifuged in a 10%-40% discontinuous sucrose gradient (Lauth et al., 1976) to purify macronuclei. The resulting macronuclear preparation was pelleted by centrifugation at 4000 × g, washed in 50ml TMS buffer (10mM Tris pH 7.5, 10mM $MgCl_2$, 3mM $CaCl_2$, 0.25M sucrose), resuspended in a final volume of 300μL, and equilibriated at 37°C for 5 min. Chromatin was then digested with MNase (New England Biolabs) at a final concentration of 15.7 Kunitz Units / μL at 37°C for 1 min 15 sec, 3 min, 5 min, 7 min 30sec, 10 min 30 sec, and 15 min respectively. Reactions were stopped by adding ½ volume of PK buffer (300mM NaCl, 30mM Tris pH 8, 75mM EDTA pH 8, 1.5% w/v SDS, 0.5mg/mL Proteinase K). Each sample was incubated at 65°C overnight to reverse crosslinks and deproteinate samples. Subsequently, nucleosomal DNA was purified through phenol:chloroform:isoamyl alcohol extraction and ethanol precipitation. Each sample was loaded on a 2% agarose-TAE gel to check the extent of MNase digestion. The sample exhibiting ~80% mononucleosomal species was selected for MNase-seq analysis, in accordance with previous guidelines (Zhang and Pugh, 2011). Mononucleosome-sized DNA was gel-purified using a QIAquick gel extraction kit (QIAGEN). Illumina libraries were prepared using an NEBNext Ultra II DNA Library Prep Kit (New England Biolabs) and subjected to paired-end sequencing on an Illumina HiSeq 2500 according to manufacturer's instructions. All vegetative *Tetrahymena* MNase-seq data were obtained from (Beh et al., 2015).

poly(A)+ RNA-seq and TSS sequencing—*Oxytricha* cells were lysed in TRIzol reagent (Thermo Fisher Scientific) for total RNA isolation according to manufacturer's instructions. Poly(A)+ RNA was then purified using the NEBNext Poly(A) mRNA Magnetic Isolation Module (New England Biolabs). *Oxytricha* poly(A)+ RNA was prepared for RNA-seq using the ScriptSeq v2 RNA-Seq Library Preparation Kit (Illumina). *Tetrahymena* poly(A)+ RNA-seq data was obtained from (Xiong et al., 2012). The 5' ends of capped RNAs were enriched from vegetative *Oxytricha* total RNA using the RAMPAGE protocol (Batut et al., 2013), and used for library preparation, Illumina sequencing and subsequent transcription start site determination (ie. "TSS-seq"). These data were used to plot the distribution of *Oxytricha* TSS positions in Figure 1A. TSS positions used for analysis outside of Figure 1A were obtained from (Swart et al., 2013) and (Beh et al., 2015).

For RNAseq analysis of genes grouped according to "starting" methylation level level: total 6mA was counted between 100 bp upstream to 250 bp downstream of the TSS. Genes with high starting methylation have total 6mA in the 90th percentile and higher. Genes with low starting methylation have total 6mA at or below the 10th percentile.

Immunoprecipitation and Illumina sequencing of methylated DNA (6mA IP-seq)—Genomic DNA was isolated from vegetative *Oxytricha* cells using the Nucleospin Tissue Kit (Takara Bio USA, Inc.). DNA was sheared into 150bp fragments using a Covaris LE220 ultra-sonicator (Covaris). Samples were gel-purified on a 2% agarose-TAE gel, blunted with DNA polymerase I (New England Biolabs), and purified using MinElute spin columns (QIAGEN). The fragmented DNA was dA-tailed using Klenow Fragment (3′ -> 5′ exo-) (New England Biolabs) and ligated to Illumina adaptors following manufacturer's instructions. Subsequently, 2.2μg of adaptor-ligated DNA containing 6mA was immunoprecipitated using an anti-N6-methyladenosine antibody (Cedarlane Labs) conjugated to Dynabeads Protein A (Invitrogen). The anti-6mA antibody is commonly used for RNA applications, but has also been demonstrated to recognize 6mA in DNA (Fioravanti et al., 2013; Xiao and Moore, 2011). The immunoprecipitated and input libraries were treated with proteinase K, extracted with phenol:chloroform, and ethanol precipitated. Finally, they were PCR-amplified using Phusion Hot Start polymerase (New England Biolabs) and used for Illumina sequencing.

Sample preparation for SMRT-seq—Vegetative *Oxytricha* macronuclei were isolated as described in the subheading "*in vivo* MNase-seq" of this study. Vegetative *Tetrahymena* macronuclei were isolated by differential centrifugation (Beh et al., 2015). *Oxytricha* and *Tetrahymena* cells were not fixed prior to nuclear isolation. Genomic DNA was isolated from *Oxytricha* and *Tetrahymena* macronuclei using the Nucleospin Tissue Kit (Macherey-Nagel). Alternatively, whole *Oxytricha* cells instead of macronuclei were used. SMRT-seq according to manufacturer's instructions, using P5-C3 and P6-C4 chemistry, as in (Chen et al., 2014),. *Oxytricha* and *Tetrahymena* macronuclear DNA were used for SMRT-seq in Figures 1 and S2A–F, while *Oxytricha* whole cell DNA was used for all other Figures. Since almost all DNA in *Oxytricha* cells is derived from the macronucleus (Prescott, 1994), similar results are expected between the use of purified macronuclei or whole cells.

Illumina data processing—Reads from all biological replicates were merged before downstream processing. All Illumina sequencing data were quality trimmed (minimum quality score = 20) and length-filtered (minimum read length = 40nt) using Galaxy (Blankenberg et al., 2010; Giardine et al., 2005; Goecks et al., 2010). MNase-seq and 6mA IP-seq reads were mapped to complete chromosomes in the *Oxytricha trifallax* JRB310 (August 2013 build) or *Tetrahymena* thermophila SB210 macronuclear reference genomes (June 2014 build) using Bowtie2 (Langmead and Salzberg, 2012) with default settings, while poly(A)+ RNA-seq and TSS-seq reads were mapped using TopHat2 (Mortazavi et al., 2008) with August 2013 *Oxytricha* gene models or June 2014 *Tetrahymena* gene models, with default settings.

MNase-seq datasets were generated by paired-end sequencing. Within each MNase-seq dataset, the read pair length of highest frequency was identified. All read pairs with length +/

− 25bp from this maximum were used for downstream analysis. On the other hand, 6mA IP-seq datasets were generated by single-read sequencing. 6mA IP-seq single-end reads were extended to the mean fragment size, computed using cross-correlation analysis (Kharchenko et al., 2008). The per-basepair coverage of *Oxytricha* MNase-seq read pair centers and extended 6mA IP-seq reads were respectively computed across the genome. Subsequently, the per-basepair coverage values were normalized by the average coverage within each chromosome to account for differences in DNA copy number (and hence, read depth) between *Oxytricha* chromosomes (Swart et al., 2013). The per-basepair coverage values were then smoothed using a Gaussian filter of standard deviation = 15. This smoothed data is denoted as "normalized coverage" or "nucleosome occupancy". *Tetrahymena* MNase-seq data were processed similarly to *Oxytricha*, except that DNA copy number normalization was omitted as *Tetrahymena* chromosomes have uniform copy number (Eisen et al., 2006).

For the MNase-seq analysis in Figures 4C, 6E, S7A, and S7B, nucleosome occupancy and 6mA IP-seq coverage were calculated within overlapping 51bp windows across the 98 assayed chromosomes. Windows were binned according to the number of 6mA residues within. The *in vitro* MNase-seq coverage from chromatinized native gDNA ("+" 6mA) was divided by the corresponding coverage from chromatinized minigenome DNA ("−" 6mA) to obtain the fold change in nucleosome occupancy in each window. Alternatively, a subtraction was performed on these datasets to obtain the difference in nucleosome occupancy *in vitro*. Identical DNA sequences were compared for each calculation. These data are labeled as ("+" histones) in Figures 4C and S7A. Naked native gDNA and mini-genome DNA were also MNase-digested, sequenced and analyzed in the same manner to control for MNase sequence preferences ("−" histones). Nucleosome occupancy *in vivo* corresponds to normalized MNase-seq coverage from wild type and *mta1* mutant cells.

Nucleosome positions were iteratively called as local maxima in normalized MNase-seq coverage, as previously described (Beh et al., 2015). "Consensus" +1, +2, +3 nucleosome positions downstream of the TSS were inferred from aggregate MNase-seq profiles across the genome (Figure 1A for *Oxytricha* and Figure S2A for *Tetrahymena*). Each gene was classified as having a +1, +2, +3 and/or +4 nucleosome if there is a called nucleosome dyad within 75 bp of the consensus nucleosome position.

RNA-seq and TSS-seq read coverage were calculated without normalization by DNA copy number since there is no correlation between *Oxytricha* DNA and transcript levels (Swart et al., 2013).

Oxytricha TSSs were called from TSS-seq data using CAGEr (Haberle et al., 2015); with clusterCTSS parameters (threshold = 1.6, thresholdIsTpm = TRUE, nrPassThreshold = 1, method = "paraclu", removeSingletons = TRUE, keepSingletonsAbove = 5). Only TSSs with tags per million counts > 0.1 were used for downstream analysis. *Tetrahymena* TSSs were obtained from (Beh et al., 2015).

SMRT-seq data processing—We processed SMRT-seq data with SMRTPipe v1.87.139483 in the SMRT Analysis 2.3.0 environment using, in order, the P_Fetch, P_Filter (with minLength = 50, minSubreadLength = 50, readScore = 0.75, and artifact = −1000),

P_FilterReports, P_Mapping (with gff2Bed = True, pulsemetrics = DeletionQV, IPD, InsertionQV, PulseWidth, QualityValue, MergeQV, SubstitutionQV, DeletionTag, and loadPulseOpts = byread), P_MappingReports, P_GenomicConsensus (with algorithm = quiver, outputConsensus = True, and enableMapQVFilter = True), P_ConsensusReports, and P_ModificationDetection (with identifyModifcations = True, enableMapQVFilter = False, and mapQvThreshold = 10) modules. All other parameters were set to the default. The *Oxytricha* August 2013 reference genome build was used for mapping *Oxytricha* SMRT-seq reads, with Contig10040.0.1, Contig1527.0.1, Contig4330.0.1, and Contig54.0.1 removed, as they are perfect duplicates of other Contigs in the assembly. *Tetrahymena* SMRT-seq reads were mapped to the June 2014 reference genome build. Only chromosomes with high SMRT-seq coverage (>= 80× for *Oxytricha*; >=100× for *Tetrahymena*) were used for all 6mA-related analyses.

Chromosome synthesis—Synthetic Contig1781.0 chromosomes were constructed from "building blocks" of native chromosome sequence (Figures 5B and 5C). The dark blue building block in Figure 5B was prepared by annealing synthetic oligonucleotides, while all other building blocks were generated by PCR-amplification from genomic DNA using Phusion DNA polymerase (New England Biolabs). All oligonucleotides used for annealing and PCR amplification are listed in Table S6. The PCR-amplified building blocks contain terminal restriction sites for *BsaI* (New England Biolabs), a type IIS restriction enzyme that cuts distal from these sites. *BsaI* cleaves within the native DNA sequence, generating custom 4nt 5' overhangs and releasing the non-native *BsaI* restriction site as small fragments that are subsequently purified away. The *BsaI*-generated overhangs are complementary only between adjacent building blocks, conferring specificity in ligation and minimizing undesired by-products. After *BsaI* digestion, PCR building blocks were purified by phenol:chloroform extraction and ethanol precipitation. Building blocks were then sequentially ligated to each other using T4 DNA ligase (New England Biolabs) and purified by phenol:chloroform extraction and ethanol precipitation. Size selection after each ligation step was performed using polyethylene glycol (PEG) precipitation or Ampure XP beads (Beckman Coulter) to enrich for the large ligated product over its smaller constituents. The size of individual building blocks and their corresponding order of ligation were designed to maximize differences in size between ligated products and individual building blocks. This increases the efficiency in size selection of products over reactants. Chromosomes 1 and 6 in Figure 5B was generated by full length PCR from genomic DNA. To prepare chromosomes 2-4 in Figure 5B, the red, dark blue, and purple blocks were first ligated in a 3-piece reaction and purified from the individual components. This product was subsequently ligated with the turquoise building block to obtain the full length chromosome. To prepare chromosomes 5 in Figure 5B, the red, orange, and emerald building blocks were ligated in a 3-piece reaction and subsequently purified. All chromosomes were subjected to Sanger sequencing to verify ligation junctions. 6mA was installed in synthetic chromosomes using annealed oligonucleotides, or by incubation of DNA building blocks with *EcoGII* methyltransferase (New England Biolabs).

Verification of synthetic chromosome sequences—All chromosomes were dA-tailed using Klenow Fragment (3′ -> 5′ exo-) (New England Biolabs), cloned using a

TOPO TA cloning kit (Thermo Fisher) or StrataClone PCR Cloning Kit (Agilent Technologies), transformed into One Shot TOP10 chemically competent *E. coli*, and sequenced using flanking T7, T3, M13F, or M13R primers.

Preparation of *Oxytricha* histones—Vegetative *Oxytricha trifallax* strain JRB310 was cultured as described in the subheading: "Experimental model and subject details" of this study. Cells were starved for 14 hr and subsequently harvested for macronuclear isolation as described in the subheading: "*in vivo* MNase-seq" of this study. However, formaldehyde fixation was omitted. Purified nuclei were pelleted by centrifugation at 4000 × g, resuspended in 0.421mL 0.4N H_2SO_4 per 10^6 input cells, and nutated for 3 hr at 4°C to extract histones. Subsequently, the acid-extracted mixture was centrifuged at 21,000 × g for 15 min to remove debris. Proteins were precipitated from the cleared supernatant using trichloroacetic acid (TCA), washed with cold acetone, then dried and resuspended in 2.5% v/v acetic acid. Individual core histone fractions were purified from crude acid-extracts using semi-preparative RP-HPLC (Vydac C18, 12 micron, 10 mM × 250 mm) with 40-65% HPLC solvent B over 50 min (Figure S6A). The identity of each purified histone fraction was verified by western analysis (Figure S6C) using antibodies: anti-H2A (Active Motif #39111), anti-H2B (Abcam #ab1790), anti-H3 (Abcam #ab1791), anti-H4 (Active Motif #39269).

Preparation of recombinant *Xenopus* histones—All RP-HPLC analyses were performed using 0.1% TFA in water (HPLC solvent A), and 90% acetonitrile, 0.1% TFA in water (HPLC solvent B) as the mobile phases. Wild-type *Xenopus* H4, H3 C110A, H2B and H2A proteins were expressed in BL21(DE3) pLysS *E.coli* and purified from inclusion bodies through ion exchange chromatography (Debelouchina et al., 2016). Purified histones were characterized by ESI-MS using a MicrOTOF-Q II ESI-Qq-TOF mass spectrometer (Bruker Daltonics). H4: calculated 11,236 Da, observed 11,236.1 Da; H3 C110A: calculated 15,239 Da, observed 15,238.7 Da; H2A: calculated 13,950 Da, observed 13,949.8 Da; H2B: calculated 13,817 Da, observed 13,816.8 Da.

Preparation of histone octamers—*Oxytricha* and *Xenopus* histone octamers were respectively refolded from core histones using established protocols (Beh et al., 2015; Debelouchina et al., 2016). Briefly, lyophilized histone proteins (*Xenopus* modified or wild-type; *Oxytricha* acid-extracted) were combined in equimolar amounts in 6 M guanidine hydrochloride, 20 Mm Tris pH 7.5 and the final concentration was adjusted to 1mg/mL. The solution was dialyzed against 2M NaCl, 10mM Tris, 1mM EDTA, and the octamers were purified from tetramer and dimer species using size-exclusion chromatography on a Superdex 200 10/300 column (GE Healthcare Life Sciences). The purity of each fraction was analyzed by SDS-PAGE. Pure fractions were combined, concentrated and stored in 50% v/v glycerol at −20°C.

Preparation of mini-genome DNA—98 full-length chromosomes were individually amplified from *Oxytricha trifallax* strain JRB310 genomic DNA using Phusion DNA polymerase (New England Biolabs). Primer pairs are listed in Table S6. Amplified chromosomes were separately purified using a MinElute PCR purification kit (QIAGEN),

and then mixed in equimolar ratios to obtain “mini-genome” DNA. The sample was concentrated by ethanol precipitation and adjusted to a final concentration of ~1.6mg/mL.

Preparation of native genomic DNA for chromatin assemblystarry—Macronuclei were isolated from vegetative *Oxytricha trifallax* strain JRB310 as described in the subheading “*in vivo* MNase-seq” of this study. However, cells were not fixed prior to nuclear isolation. Genomic DNA was purified using the Nucleospin Tissue kit (Macherey-Nagel). Approximately 200μg of genomic DNA was loaded on a 15%-40% linear sucrose gradient and centrifuged in a SW 40 Ti rotor (Beckman Coulter) at 160,070 × g for 22.5hr at 20°C. Sucrose solutions were in 1M NaCl, 20mM Tris pH 7.5, 5mM EDTA. Individual fractions from the sucrose gradient were analyzed on 0.9% agarose-TAE gels. Fractions containing high molecular weight DNA that migrated at the mobility limit were discarded as such DNA species were found to interfere with downstream chromatin assembly. All other fractions were pooled, ethanol precipitated, and adjusted to 0.5mg/mL DNA.

Chromatin assembly and preparation of mononucleosomal DNA—Chromatin assemblies were prepared by salt gradient dialysis as previously described (Beh et al., 2015; Luger et al., 1999), or using mouse NAP1 histone chaperone and *Drosophila* ACF chromatin remodeler as previously described (An and Roeder, 2003; Fyodorov and Kadonaga, 2003). Details of each chromatin assembly procedure are listed below. To reduce sample requirements while maintaining adequate DNA concentrations for chromatin assembly, synthetic chromosomes were first mixed with a hundred-fold excess of “buffer” DNA (PCR-amplified *Oxytricha* Contig17535.0). We verified that nucleosome occupancy in the methylated region (qPCR primer pairs 6 and 7) of the synthetic chromosome is unaffected by the presence of buffer DNA (Figure S7E). Native and mini-genome DNA were not mixed with buffer DNA prior to chromatin assembly.

For chromatin assembly through salt dialysis: histone octamers and (synthetic chromosome + buffer) DNA were mixed in a 0.8:1 mass ratio, while histone octamers and (native or mini-genome) DNA were mixed in a 1.3:1 mass ratio, each in a 50μL total volume. Samples were first dialyzed into start buffer (10mM Tris pH 7.5, 1.4M KCl, 0.1mM EDTA pH 7.5, 1mM DTT) for 1 hr at 4°C. Then, 350mL end buffer (10mM Tris pH 7.5, 10mM KCl, 0.1mM EDTA, 1mM DTT) was added at a rate of 1mL/min with stirring. The assembled chromatin was dialyzed overnight at 4°C into 200mL end buffer, followed by a final round of dialysis in fresh 200mL end buffer for 1 hr at 4°C. The assembled chromatin was then adjusted to 50mM Tris pH 7.9, 5mM $CaCl_2$ and digested with MNase (New England Biolabs) to mainly mononucleosomal DNA as previously described (Beh et al., 2015).

For chromatin assembly using mouse NAP1 and *Drosophila* ACF: NAP1 was recombinantly expressed and purified as described in (An and Roeder, 2003). ACF was purchased from Active Motif. 0.49μM NAP1 and 58nM histone octamer were first mixed in a 302μl reaction volume containing 62mM KCl, 1.2% w/v polyvinyl alcohol (Sigma Aldrich), 1.2% w/v polyethylene glycol 8000 (Sigma Aldrich), 25mM HEPES-KOH pH 7.5, 0.1mM EDTA-KOH, 10% v/v glycerol, and 0.01% v/v NP-40. The NAPI-histone mix was incubated on ice for 30 min. Meanwhile, “AM” mix was prepared, consisting of 20mM ATP (Sigma Aldrich), 200mM creatine phosphate (Sigma Aldrich), 33.3mM $MgCl_2$, 33.3μg/μl creatine kinase

(Sigma Aldrich) in a 56µl reaction volume. After the 30 min incubation, 5.29 µl of 1.7 µM ACF complex (Active Motif) and the "AM" mix were sequentially added to the NAP1-histone mix. Then, 10.63µl of native or mini-genome DNA (2.66µg) was added, resulting in a 374µl reaction volume. The final mixture was incubated at 27°C for 2.5 hr to allow for chromatin assembly. Subsequently, $CaCl_2$ was added to a final concentration of 5mM, and the chromatin was digested with MNase (New England Biolabs) to mainly mononucleosomal DNA as previously described (Beh et al., 2015).

Mononucleosome-sized DNA from MNase-digested chromatin was gel-purified and used for tiling qPCR on a Viia 7 Real-Time PCR System with Power SYBR Green PCR master mix (Thermo Fisher), or *in vitro* MNase-seq on an Illumina HiSeq 2500, according to the manufacturer's instructions. qPCR primer sequences are listed in Table S6.

Tiling qPCR analysis of nucleosome occupancy—qPCR data were analyzed using the ΔΔCt method (Livak and Schmittgen, 2001). At each locus along the synthetic chromosome, ΔCt = (Ct at locus of interest) – (Ct at qPCR primer pair 22, far from the methylated region). See Figure 6B for location of qPCR primer pair 22. Separate ΔCt values were calculated from mononucleosomal DNA and the corresponding naked, undigested synthetic chromosome. The ΔΔCt value was calculated from this pair of ΔCt values. This controls for potential variation in PCR amplification efficiency, especially over methylated regions. The fold change in mononucleosomal DNA relative to naked chromosomal DNA at a particular locus is calculated as $2^{-\Delta\Delta Ct}$, and denotes 'nucleosome occupancy' for all presented qPCR data.

ACF spacing assay—ATP-dependent nucleosome spacing was performed in accordance with a previous study (Lieleg et al., 2015). Chromatin was assembled by salt gradient dialysis as described above, and then adjusted to 20mM HEPES-KOH pH 7.5, 80mM KCl, 0.5mM EGTA, 12% v/v glycerol, 10mM $(NH_4)_2SO_4$, 2.5mM DTT. Samples were then incubated for 2.5 hr at 27°C with 3mM ATP, 30mM creatine phosphate, 4mM $MgCl_2$, 5 ng/µl creatine kinase, and 11 ng/µL ACF complex (Active Motif). Remodeled chromatin was then adjusted to 5mM $CaCl_2$ and subjected to MNase digestion, mononucleosomal DNA purification, and qPCR analysis as described above.

Phylogenetic analysis—The MTA1 amino acid sequence (UniProt ID: J9IF92_9SPIT) was queried against the NCBI nr database using PSI-BLAST (Altschul et al., 1997; Schäffer et al., 2001) (maximum e-value = $1e^{-4}$; enable short queries and filtering of low complexity regions). Retrieved hits were collapsed using CD-HIT (Huang et al., 2010) with minimum sequence identity = 0.97 to remove redundant sequences. The resulting sequences were added to existing MT-A70 alignments from (Greer et al., 2015) using MAFFT (--add) (Katoh et al., 2017; Kuraku et al., 2013). Gaps and duplicate sequences were removed from the merged alignment. Only sequences corresponding to the taxa in Figure 2B were retained. The alignment was then used for phylogenetic tree construction using MrBayes in the CIPRES Science Gateway (Miller et al., 2010) with 5×10^6 generations. Protein sequences used for MrBayes analysis are given in Table S5.

The above procedure was also used for constructing phylogenetic trees from p1 (UniProt ID: Q22VV9_TETTS) and p2 (UniProt ID: I7M8B9_TETTS). However, protein sequences were aligned using MAFFT without adding to an existing alignment.

Preparation of nuclear extracts with DNA methyltransferase activity—Vegetative *Tetrahymena* cells were grown in SSP medium to log-phase (~3.5×10^5 cells/mL) and collected by centrifugation at 2,300 × g for 5 min in an SLA-3000 rotor. The supernatant was discarded, and cells were resuspended in medium B (10mM Tris pH 6.75, 2mM $MgCl_2$, 0.1M sucrose, 0.05% w/v spermidine trihydrochloride, 4% w/v gum Arabic, 0.63% w/v 1-octanol, and 1mM PMSF). Gum arabic (Sigma Aldrich) is prepared as a 20% w/v stock and centrifuged at 7,000 × g for 30 min to remove undissolved clumps. For each volume of cell culture, one-third volume of medium B was added to the *Tetrahymena* cell pellet. Cells were resuspended and homogenized in a chilled Waring Blender (Waring PBB212) at high speed for 40 sec. The resulting lysate was subsequently centrifuged at 2,750 × g for 5 min in an SLA-3000 rotor to pellet macronuclei. The nuclear pellet was washed twice with medium B and then five times in MM medium (10mM Tris-HCl pH 7.8, 0.25M sucrose, 15mM $MgCl_2$, 0.1% w/v spermidine trihydrochloride, 1mM DTT, 1mM PMSF). Macronuclei were pelleted between wash steps by centrifuging at 2,500 × g for 5 min in an SLA-3000 rotor. Finally, the total number of washed macronuclei was counted with a hemocytometer using a Zeiss ID03 microscope. Nuclear proteins were extracted by vigorously resuspending the pellet in MMsalt buffer (10mM Tris-HCl pH 7.8, 0.25M sucrose, 15mM $MgCl_2$, 350mM NaCl, 0.1% w/v spermidine trihydrochloride, 1mM DTT, 1mM PMSF). 1mL MMsalt buffer was added per 2.33×10^8 macronuclei. The viscous mixture was nutated for 45 min at 4°C, and then cleared at 175,000 × g for 30 min at 4°C in a SW 41 Ti rotor. Following this, the supernatant was dialyzed in a Slide-A-Lyzer 3.5K MWCO cassette (Thermo Fisher) overnight at 4°C against two changes of MMminus medium (10mM Tris-HCl pH 7.8, 15mM $MgCl_2$, 1mM DTT, 0.5mM PMSF). The dialysate was then centrifuged at 7,197 × g for 1 hr at 4°C to remove precipitates, and dialyzed overnight in a Slide-A-Lyzer 3.5K MWCO cassette (Thermo Fisher) at 4°C against two changes of MN3 buffer (30mM Tris-HCl pH 7.8, 1mM EDTA, 15mM NaCl, 20% v/v glycerol, 1mM DTT, 0.5mM PMSF). The final dialysate was cleared by centrifugation at 7,197g for 1.5 hr at 4°C, flash frozen, and stored at −80°C. This nuclear extract was used for all subsequent biochemical fractionation and 6mA methylation assays.

Partial purification of MTA1c from nuclear extracts—*Tetrahymena* nuclear extracts were passed through a HiTrap Q HP column (GE Healthcare) and eluted using a linear gradient of 15mM to 650mM NaCl in 30mM Tris-HCl pH 7.8, 1mM EDTA, 20% v/v glycerol, 1mM DTT, 0.5 mM PMSF, over 30 column volumes. Each fraction was assayed for DNA methyltransferase activity using radiolabeled SAM as described in the next section. The DNA methyltransferase activity eluted in two peaks, at ~60mM and ~365mM NaCl, termed the “low salt sample” and “high salt sample”. Fractions corresponding to each peak were pooled and passed through a HiTrap Heparin HP column (GE Healthcare). Bound proteins were eluted using a linear gradient of 60 mM to 1M NaCl (for the low salt sample) or 350mM to 1M NaCl (for the high salt sample) over 30 column volumes. Fractions with DNA methyltransferase activity were respectively pooled and dialyzed into 10mM sodium

phosphate pH 6.8, 100mM NaCl, 10% v/v glycerol, 0.3mM $CaCl_2$, 0.5mM DTT (for the low salt sample); or 30mM Tris-HCl pH 7.8, 1mM EDTA, 200mM NaCl, 10% v/v glycerol, 1mM DTT, 0.2mM PMSF (for the high salt sample). The dialyzed low salt sample was passed through a Nuvia cPrime column (Bio-Rad) and eluted using a linear gradient of 100 mM to 1M NaCl in 50 mM sodium phosphate pH 6.8, 10% v/v glycerol, 0.5 mM DTT. Separately, the dialyzed high salt sample was fractionated using a Superdex 200 10/300 GL column (GE Healthcare) in 30mM Tris-HCl pH 7.8, 1mM EDTA, 200mM NaCl, 10% v/v glycerol, 1mM DTT. Fractions from the Nuvia cPrime and Superdex 200 columns were dialyzed into 30mM Tris-HCl pH 7.8, 1mM EDTA, 15mM NaCl, 20% v/v glycerol, 1mM DTT, 0.5mM PMSF and assayed for DNA methyltransferase activity. Those with qualitatively low, medium, and high activity were subjected to mass spectrometry to identify candidate methyltransferase proteins (Figure 2D and Table S3). This experiment identified four proteins that co-purify with DNA methyltransferase activity – MTA1, MTA9, p1, and p2 – and are collectively termed as “MTA1c” in our study. All four proteins are necessary for 6mA methylation *in vitro*.

Recombinant expression of MTA1, MTA9, p1, and p2 proteins—Full length MTA1, MTA9, p1, and p2 open reading frames were codon-optimized for bacterial expression and cloned into a pET-His6-SUMO vector using ligation independent cloning. Protein sequences are listed in Table S7. The vector was a gift from Scott Gradia (Addgene plasmid #29659; http://n2t.net/addgene:29659; RRID: Addgene_29659). Mutations in the MTA1 open reading frame was introduced using the Q5® Site-Directed Mutagenesis Kit (New England Biolabs). For recombinant expression, pET-His6-SUMO-MTA1 (wild type and mutant) was transformed into SHuffle T7 competent *E. coli* (New England Biolabs); pET-His6-SUMO-MTA9 was transformed into Lemo (DE3) competent *E. coli* (New England Biolabs); pET-His6-SUMO-p1 and pET-His6-SUMO-p2 were transformed into BL21(DE3) competent *E. coli* (New England Biolabs). IPTG induction was performed at 16°C overnight. Induced cells were resuspended in 25ml of lysis buffer B (50mM Tris pH 7.8, 300mM NaCl, 5% v/v glycerol, 10mM imidazole, 5mM BME, 1mM PMSF, 0.5× ProBlock Gold Bacterial protease inhibitor cocktail [GoldBio]). The cells were sonicated at 35% amplitude for a total of 4 minutes, with a 10 sec off, 10 sec cycle using a Model 505 Sonic Dismembrator (Fisherbrand). Lysates were cleared by centrifugation at 30,000g for 30 min at 4°C, mixed with pre-washed Ni-NTA agarose (Invitrogen), and nutated for 45min at 4°C. The resin was subsequently washed with lysis buffer and eluted in 50mM Tris pH 7.8, 300mM NaCl, 5%v/v glycerol, 400mM glycerol, 5mM BME, 1× ProBlock Gold bacterial protease inhibitor cocktail [GoldBio]). Eluates were dialyzed into lysis buffer B and then digested with TEV protease (gift from S.H. Sternberg) at 4°C overnight. The resulting mixture was passed through a fresh batch of Ni-NTA agarose (Invitrogen) to remove cleaved affinity tags. The flow-through containing each recombinant protein was flash frozen and used for all downstream methyltransferase assays.

Methyltransferase assays

Generation of DNA and RNA substrates: A 954bp dsDNA PCR product was used in all assays involving *Tetrahymena* nuclear extract. This substrate was amplified by PCR from *Tetrahymena thermophila* strain SB210 macronuclear SB210 genomic DNA using PCR

primers metGATC_F2 and metGATC_R2 (Table S6). The resulting product was purified using Ampure XP beads (Beckman Coulter). This 954bp region of the genome contains a high level of 6mA *in vivo*. Thus, the underlying DNA sequence may be intrinsically amenable to methylation by *Tetrahymena* MTA1. Note that the amplified 954bp product is devoid of DNA methylation as unmodified dNTPs were used for PCR. Separately, a 350bp dsDNA PCR product was used in all assays involving recombinant MTA1, MTA9, p1 and p2. This sequence lacks 5'-NATC-3' motifs, and was used to reduce background DNA methylation from contaminating *Dam* methyltransferase in recombinant protein preparations. The 350bp dsDNA PCR product was amplified from *Tetrahymena thermophila* strain SB210 macronuclear SB210 genomic DNA using the PCR primers noGATC2_F and noGATC2_R (Table S6), and purified using Ampure XP beads (Beckman Coulter).

For short DNA substrates (< 50bp), oligonucleotides were purchased from Integrated DNA Technologies and either directly used as ssDNA, or annealed with its complementary sequence to obtain dsDNA. To prepare hemimethylated 27bp dsDNA in Figure 2G, either strand was methylated using *EcoGII* methyltransferase (New England BioLabs) before annealing with the complementary sequence.

To generate ~350nt ssRNA and ~350bp dsRNA, the aforementioned 350bp dsDNA was first PCR-amplified using primers containing T7 overhangs (primer pairs T7noGATC2_F2 / noGATC2_R and T7noGATC2_F2 / T7noGATC2_R2 respectively; see Table S6 for primer sequences). Each PCR product was used as a template for *in vitro* transcription using the HiScribe T7 High Yield RNA Synthesis Kit (New England Biolabs). The synthesized RNA was rigorously treated with DNase (ThermoFisher) purified using acid phenol:chloroform extraction, followed by two rounds of chloroform extraction. Each sample was subsequently ethanol precipitated and resuspended in water for use in methyltransferase assays.

Radioactive methyltransferase assay: For experiments involving nuclear extract, 2.18μg of 954bp dsDNA substrate was mixed with 4-8μl nuclear extract and 0.64μM ^{3}H-labeled S-adenosyl-L-methionine ([^{3}H]SAM) in 33mM Tris-HCl pH 7.5, 6mM EDTA, 4.3mM BME, in a 15μl reaction volume. For experiments involving recombinant MTA1c protein components (ie. MTA1, MTA9, p1, and/or p2), ~3μM oligonucleotide ssDNA / annealed dsDNA is used. Alternatively, 1.3μg of 350bp dsDNA substrate (or an equimolar amount ~350nt ssRNA, or ~350bp dsDNA) was used in place of DNA oligonucleotide substrates. ssRNA was heated at 90°C for 2 min and snap cooled to minimize secondary structures before mixing with other components of the methyltransferase assay. All samples were incubated overnight at 37°C, and subsequently spotted onto 1cm × 1cm squares of Hybond-XL membrane (GE Healthcare). Membranes were then washed thrice with 0.2M ammonium bicarbonate, once with distilled water, twice with 100% ethanol, and finally air-dried for 1 hr. Each membrane was immersed in 5mL Ultima Gold (PerkinElmer) and used for scintillation counting on a TriCarb 2910 TR (PerkinElmer).

Non-radioactive methyltransferase assay: For assays involving nuclear extract: 5.5μg of 954bp DNA substrate was mixed with 2μl nuclear extract and 0.2mM S-adenosyl-L-methionine (NEB) in 33mM Tris-HCl pH 7.5, 6mM EDTA, 4.3mM BME in a 15μl reaction volume. For assays involving recombinant MTA1c protein components (ie. MTA1, MTA9,

p1, and/or p2), 2.6μg of 350bp DNA substrate was mixed with 540nM MTA1, 90nM MTA9, 1.5μM p1, 1.0μM p2 proteins. The band of expected size in each recombinant protein preparation was compared against a series of BSA standards to calculate protein concentration. All methylation reactions were incubated at 37°C overnight, then purified using a MinElute purification kit (QIAGEN), denatured at 95°C for 10 min, and snap cooled in an ice water bath. Samples were spotted on a Hybond N+ membrane (GE Healthcare), air dried for 5 min and UV-cross-linked with 120,000 μJ / cm^2 exposure using an Ultra-Lum UVC-515 Ultraviolet Multilinker. The cross-linked membrane was blocked in 5% milk in TBST (containing 0.1% v/v Tween) and incubated with 1:1,000 anti-N6-methyladenosine antibody (Synaptic Systems) at 4°C overnight. The membrane was then washed three times with TBST, incubated with 1:3,000 Goat anti-rabbit HRP antibody (Bio-Rad) at room temperature for 1 hr, washed another three times with 1× TBST, and developed using Amersham ECL Western Blotting Detection Kit (GE Healthcare). This dot blot assay was used to measure 6mA levels in Figures 2F, 3B, 5C and S3C.

Quantitative mass spectrometry analysis of dA and 6mA—10.5μg *Oxytricha* or *Tetrahymena* macronuclear genomic DNA was first digested to nucleosides by mixing with 14μl DNA degradase plus enzyme (Zymo Research) in a 262.5μl reaction volume. Samples were incubated at 37°C overnight, then 70°C for 20 min to deactivate the enzyme.

The internal nucleoside standards $^{15}N_5$-dA and D_3-6mA were used to quantify endogenous dA and 6mA levels in ciliate DNA. $^{15}N_5$-dA was purchased from Cambridge Isotope Laboratories, while D_3-6mA was synthesized as described in the following section. Nucleoside samples were spiked with 1 ng/μl $^{15}N_5$-dA and 200 pg/μl D_3-6mA in an autosampler vial. Samples were loaded onto a 1mm × 100mm C18 column (Ace C18-AR, Mac-Mod) using a Shimadzu HPLC system and PAL auto-sampler (20μl / injection) at a flow rate of 70μl / min. The column was connected inline to an electrospray source couple to an LTQ-Orbitrap XL mass spectrometer (Thermo Fisher). Caffeine (2 pmol/μl in 50% Acetonitrile with 0.1% FA) was injected as a lock mass through a tee at the column outlet using a syringe pump at 0.5μl/min (Harvard PHD 2000). Chromatographic separation was achieved with a linear gradient from 10% to 99% B (A: 0.1% Formic Acid, B: 0.1% Formic Acid in Acetonitrile) in 5 min, followed by 5 min wash at 100% B and equilibration for 10 min with 1% B (total 20 min program). Electrospray ionization was achieved using a spray voltage of 4.50 kV aided by sheath gas (Nitrogen) flow rate of 18 (arbitrary units) and auxiliary gas (Nitrogen) flow rate of 2 (arbitrary units). Full scan MS data were acquired in the Orbitrap at a resolution of 60,000 in profile mode from the m/z range of 190-290. A parent mass list was utilized to acquire MS/MS spectra at a resolution of 7500 in the Orbitrap. LC-MS data were manually interpreted in Xcalibur's Qual browser (Thermo, Version 2.1) to visualize nucleoside mass spectra and to generate extracted ion chromatograms by using the theoretical [M+H] within a range of ±2ppm. Peak areas were extracted in Skyline (Ver. 3.5.0.9319).

Synthesis of D_3-6mA nucleoside—2′-Deoxyadenosine and CD_3I were purchased from Sigma Aldrich. Flash chromatography was performed on a Biotage Isolera using silica columns (Biotage SNAP Ultra, HP-Sphere 25μm). Semi-preparative RP-HPLC was

performed on a Hewlett-Packard 1200 series instrument equipped with a Waters XBridge BEH C18 column (5μm, 10 × 250 mm) at a flow rate of 4mL/min, eluting using A (0.1% formic acid in H2O) and B (0.1% formic acid in 9:1 MeCN/H2O). ^{1}H NMR spectra were recorded on a Bruker UltraShield Plus 500 MHz instrument. Data for ^{1}H NMR are reported as follows: chemical shift (δ ppm), multiplicity (s = singlet, br = broad signal, d = doublet, dd = doublet of doublets) and coupling constant (Hz) where possible. ^{13}C NMR spectra were recorded on a Bruker UltraShield Plus 500 MHz.

D_3-6mA (2′Deoxy-6-[*D*3]-methyladenosine) were synthesized and purified according to (Schiffers et al., 2017). After an initial purification by flash column chromatography, the methylated compounds were further purified by semipreparative RP-HPLC (linear gradient of 0% to 20% B over 30 min) affording the desired compounds in 14% and 10% yields respectively after lyophilization.

2′Deoxy-6-[*D*3]-methyladenosine: ^{1}H NMR (500 MHz, D_2O) δ 7.98 (s, 1H), 7.77 (s, 1H), 6.17 (m, 1H), 4.54 (m, 1H), 4.10 (m, 1H), 3.79 (dd, J = 12.7, 3.2 Hz, 1H), 3.71 (dd, J = 12.7, 4.3 Hz, 1H), 2.60 (m, 1H), 2.44 (ddd, J = 14.0, 6.3, 3.3 Hz, 1H).

^{13}C NMR (126 MHz, D_2O) δ 154.0, 151.5, 146.1, 138.9, 118.4, 87.3, 84.3, 71.1, 61.6, 39.2, 26.4 ppm. (Peak at 26.4 ppm appears as a broad signal. C-D coupling is not resolved).

HR-MS (ESI+): m/z calculated for $[C_{11}H_{13}D_3N_5O_3]^+$ ($[M+H]^+$): 269.1436, found 269.1421.

Mass spectrometry analysis of proteins in *Tetrahymena* nuclear extracts— Samples where topped up to 200μl with 50mM ammonium bicarbonate pH 8. TCEP was added to 5mM final concentration and left to incubate at 60°C for 10 min. 15mM chloroacetamide was then added and left to incubate in the dark at room temperature for 30 min. 1μg of Trypsin Gold (Promega) was added to each sample and incubated end-over-end at 37°C for 16 hr. An additional 0.25μg of Trypsin Gold was added and incubated end-over-end at 37°C for 3 hr. Samples were acidified by adding TFA to 0.2% final concentration, and desalted using SDB stage-tips (Rappsilber et al., 2007). Samples were dried completely in a speedvac and resuspended in 20μl of 0.1% formic acid pH 3. 5μl was injected per run using an Easy-nLC 1200 UPLC system. Samples were loaded directly onto a 45cm long 75μm inner diameter nano capillary column packed with 1.9um C18-AQ (Dr. Maisch, Germany) mated to metal emitter inline with an Orbitrap Fusion Lumos (Thermo Scientific, USA). The mass spectrometer was operated in data dependent mode with the 120,000 resolution MS1 scan (AGC 4e5, Max IT 50ms, 400-1500 m/z) in the Orbitrap followed by up to 20 MS/MS scans with CID fragmentation in the ion trap. Dynamic exclusion list was invoked to exclude previously sequenced peptides for 60 sec if sequenced within the last 30 sec, and maximum cycle time of 3 sec was used. Peptides were isolated for fragmentation using the quadrupole (1.6 Da window). ns was utilized. Ion-trap was operated in Rapid mode with AGC 2e3, maximum IT of 300 msec and minimum of 5000 ions.

Raw files were searched using Byonic (Bern et al., 2012) and Sequest HT algorithms (Eng et al., 1994) within the Proteome Discoverer 2.1 suite (Thermo Scientific, USA). 10ppm MS1 and 0.4Da MS2 mass tolerances were specified. Caramidomethylation of cysteine was used

as fixed modification, while oxidation of methionine, pyro-Glu from Gln and deamidation of asparagine were specified as dynamic modifications. Trypsin digestion with maximum of 2 missed cleavages were allowed. Files were searched against the *Tetrahymena themophila* macronuclear reference proteome (June 2014 build), supplemented with common contaminants (27,099 total entries).

Scaffold (version Scaffold_4.8.7, Proteome Software Inc., Portland, OR) was used to validate MS/MS based peptide and protein identifications. Peptide identifications were accepted if they could be established at greater than 93.0% probability. Peptide Probabilities from Sequest and Byonic were assigned by the Scaffold Local FDR algorithm. Protein identifications were accepted if they could be established at greater than 99.0% probability to achieve an FDR less than 1.0% and contained at least 3 identified peptides. Protein probabilities were assigned by the Protein Prophet algorithm (Nesvizhskii et al., 2003). Proteins that contained similar peptides and could not be differentiated based on MS/MS analysis alone were grouped to satisfy the principles of parsimony.

Generation of *mta1* mutant lines—A frameshift mutation in the MTA1 gene was created by inserting a small non-coding DNA segment immediately downstream of the MTA1 start codon (Figures 3A and S5H). This non-coding DNA segment belongs to a class of genetic elements that are normally eliminated during the sexual cycle (Chen et al., 2014). When ssRNA homologous to such DNA segments is injected into *Oxytricha* cells undergoing sexual development, the DNA is erroneously retained (Khurana et al., 2018). This results in disruption of the MTA1 open reading frame. The ectopic DNA segment is propagated through subsequent cell divisions after completion of the sexual cycle. RNAseq analysis confirmed the presence of the ectopic insertion in *mta1* mutant transcripts but not wild type controls (Figure S5H).

ssRNA was generated by *in vitro* transcription using a Hi-Scribe T7 High Yield RNA Synthesis Kit (New England Biolabs). The DNA template for *in vitro* transcription consists of the ectopic DNA segment flanked by 100-200bp cognate MTA1 sequence. Following DNase treatment, ssRNA was acid-phenol:chloroform extracted and ethanol precipitated. After precipitation, ssRNA was resuspended in nuclease-free water (Ambion) to a final concentration of 1 to 3 mg/mL for injection.

ssRNA microinjections—*Oxytricha* cells were mated by mixing 3mL of each mating type, JRB310 and JRB510, along with 6mL of fresh Pringsheim media. At 10 to 12 hr post mixing, pairs were isolated and placed in Volvic water with 0.2% bovine serum albumin (Jackson ImmunoResearch Laboratories) (Fang et al., 2012). ssRNA constructs were injected into the macronuclei of paired cells under a light microscope as previously described with DNA constructs (Nowacki et al., 2008). After injection, cells were pooled in Volvic water. At 60 to 72 hr post mixing, the pooled cells were singled out to grow clonal injected cell lines. As clonal population size grew, lines were transferred to 10 cm petri dishes and grown in Pringsheim media. Only water from the “Volvic” brand has been empirically tested in our laboratory to support *Oxytricha* growth. Similar products from other vendors have not been tested.

Survival analysis of Oxytricha *mta1* mutants—This experiment was performed in Figure 7D. Wild type or mutant *Oxytricha* cells were mixed at 0 hr to induce mating. Since not all cells enter the sexual cycle, mated cells are separated from unmated vegetative cells at 15 hr and transferred into a separate dish. The cells are allowed to rest for 12 hr to account for cell death during transfer. The number of surviving mated cells is counted from 27 hr onwards. The total cell number at each timepoint is normalized to 27 hr data to obtain the percentage survival. An increase in survival at 108 hr is observed in wild type samples because the cells have completed mating and reverted to the vegetative state, where they can proliferate and increase in number.

Quantification and statistical analysis—All statistical tests were performed in Python (v2.7.10) or R (v3.2.5), and described in the respective Figure and Table legends.

Data and Software Availability—*Oxytricha* SMRT-seq data are deposited in SRA under the accession numbers SRX2335608, SRX2335607, and GSE94421. *Tetrahymena* SMRT-seq and all *Oxytricha* Illumina data are deposited in NCBI GEO under accession number GSE94421.

Supplementary Material

Refer to Web version on PubMed Central for supplementary material.

Acknowledgments

We thank T. Srikumar and S. Kyin for assistance with nucleoside mass spectrometry; I. Pelczer for assistance with NMR measurements of nucleoside standards; W. Wang, J. Wiggins, and J. Miller for assistance with Illumina sequencing; C.D. Allis, V. Zakian, T. Bestor, S.H. Sternberg, W. Jack, R. Neme, G. Dann, K. Jani, A. Mostafavi and G. Liszczak for helpful discussions; I. Fernandez and A. Sobolevsky for discussions and access to FPLC equipment, and J. Wang, B. Dul, and F. Song for laboratory support. This work was funded by NIH grants R01-GM59708, R35-GM122555, and R01-GM109459 to L.F.L and R01-GM107047 to T.W.M.

References

Altschul SF, Madden TL, Schäffer AA, Zhang J, Zhang Z, Miller W, and Lipman DJ (1997). Gapped BLAST and PSI-BLAST: a new generation of protein database search programs. Nucleic Acids Res 25, 3389–3402. [PubMed: 9254694]

Ammermann D, Steinbrück G, Baur R, and Wohlert H (1981). Methylated bases in the DNA of the ciliate Stylonychia mytilus. Eur. J. Cell Biol 24, 154–156. [PubMed: 6786890]

An W, and Roeder RG (2003). Reconstitution and Transcriptional Analysis of Chromatin In Vitro. Methods Enzymol 377, 460–474.

Batut P, Dobin A, Plessy C, Carninci P, and Gingeras TR (2013). High-fidelity promoter profiling reveals widespread alternative promoter usage and transposon-driven developmental gene expression. Genome Res 23, 169–180. [PubMed: 22936248]

Beh LY, Müller MM, Muir TW, Kaplan N, and Landweber LF (2015). DNA-guided establishment of nucleosome patterns within coding regions of a eukaryotic genome. Genome Res 25, 1727–1738. [PubMed: 26330564]

Bern M, Kil YJ, and Becker C (2012). Byonic: Advanced Peptide and Protein Identification Software. Curr. Protoc. Bioinformatics. 13, 13.20.

Blankenberg D, Von Kuster G, Coraor N, Ananda G, Lazarus R, Mangan M, Nekrutenko A, and Taylor J (2010). Galaxy: a web-based genome analysis tool for experimentalists. Curr. Protoc. Mol. Biol 19, 19.10.1–21.

Bracht JR, Fang W, Goldman AD, Dolzhenko E, Stein EM, and Landweber LF (2013). Genomes on the edge: programmed genome instability in ciliates. Cell 152, 406–416. [PubMed: 23374338]

Bromberg S, Pratt K, and Hattman S (1982). Sequence specificity of DNA adenine methylase in the protozoan *Tetrahymena* thermophila. J. Bacteriol 150, 993–996. [PubMed: 6950932]

Brownell JE, Zhou J, Ranalli T, Kobayashi R, Edmondson DG, Roth SY, and Allis CD (1996). *Tetrahymena* histone acetyltransferase A: a homolog to yeast Gcn5p linking histone acetylation to gene activation. Cell 84, 843–851. [PubMed: 8601308]

Cassidy-Hanley DM. (2012). *Tetrahymena* in the Laboratory: Strain Resources, Methods for Culture, Maintenance, and Storage. In Methods in Cell Biology, pp. 237–276. [PubMed: 22444147]

Chen X, Bracht JR, Goldman AD, Dolzhenko E, Clay DM, Swart EC, Perlman DH, Doak TG, Stuart A, Amemiya CT, et al. (2014). The Architecture of a Scrambled Genome Reveals Massive Levels of Genomic Rearrangement during Development. Cell 158, 1187–1198. [PubMed: 25171416]

Clapier CR, and Cairns BR (2009). The biology of chromatin remodeling complexes. Annu. Rev. Biochem 78, 273–304. [PubMed: 19355820]

Cummings DJ, Tait A, and Goddard JM (1974). Methylated bases in DNA from Paramecium aurelia. Biochim. Biophys. Acta - Nucleic Acids Protein Synth 374, 1–11.

Debelouchina GT, Gerecht K, and Muir TW (2016). Ubiquitin utilizes an acidic surface patch to alter chromatin structure. Nat. Chem. Biol 13, 105–110. [PubMed: 27870837]

Eisen JA, Coyne RS, Wu M, Wu D, Thiagarajan M, Wortman JR, Badger JH, Ren Q, Amedeo P, Jones KM, et al. (2006). Macronuclear genome sequence of the ciliate *Tetrahymena* thermophila, a model eukaryote. PLoS Biol 4, e286. [PubMed: 16933976]

Eng JK, McCormack AL, and Yates JR (1994). An approach to correlate tandem mass spectral data of peptides with amino acid sequences in a protein database. J. Am. Soc. Mass Spectrom 5, 976–989. [PubMed: 24226387]

Engel JD, and von Hippel PH (1978). Effects of methylation on the stability of nucleic acid conformations. Studies at the polymer level. J. Biol. Chem 253, 927–934. [PubMed: 621212]

Fang W, Wang X, Bracht JR, Nowacki M, and Landweber LF (2012). Piwi-interacting RNAs protect DNA against loss during *Oxytricha* genome rearrangement. Cell 151, 1243–1255. [PubMed: 23217708]

Finn RD, Clements J, Arndt W, Miller BL, Wheeler TJ, Schreiber F, Bateman A, and Eddy SR (2015). HMMER web server: 2015 update. Nucleic Acids Res 43, W30–8. [PubMed: 25943547]

Fioravanti A, Fumeaux C, Mohapatra SS, Bompard C, Brilli M, Frandi A, Castric V, Villeret V, Viollier PHP, Biondi EEG, et al. (2013). DNA Binding of the Cell Cycle Transcriptional Regulator GcrA Depends on N6-Adenosine Methylation in Caulobacter crescentus and Other Alphaproteobacteria. PLoS Genet 9, e1003541. [PubMed: 23737758]

Fu Y, Luo G-Z, Chen K, Deng X, Yu M, Han D, Hao Z, Liu J, Lu X, Doré LC, et al. (2015). N6-methyldeoxyadenosine marks active transcription start sites in Chlamydomonas. Cell 161, 879–892. [PubMed: 25936837]

Fyodorov DV, and Kadonaga JT (2003). Chromatin assembly *in vitro* with purified recombinant ACF and NAP-1. Methods Enzymol 371, 499–515. [PubMed: 14712724]

Giardine B, Riemer C, Hardison RC, Burhans R, Elnitski L, Shah P, Zhang Y, Blankenberg D, Albert I, Taylor J, et al. (2005). Galaxy: a platform for interactive large-scale genome analysis. Genome Res 15, 1451–1455. [PubMed: 16169926]

Goecks J, Nekrutenko A, and Taylor J (2010). Galaxy: a comprehensive approach for supporting accessible, reproducible, and transparent computational research in the life sciences. Genome Biol 11, R86. [PubMed: 20738864]

Gorovsky MA, Hattman S, and Pleger GL (1973). (6 N)methyl adenine in the nuclear DNA of a eucaryote, *Tetrahymena* pyriformis. J. Cell Biol 56, 697–701. [PubMed: 4631666]

Gottschling DE, and Cech TR (1984). Chromatin structure of the molecular ends of *Oxytricha* macronuclear DNA: phased nucleosomes and a telomeric complex. Cell 38, 501–510. [PubMed: 6432344]

Greer EL, Blanco MA, Gu L, Sendinc E, Liu J, Aristizábal-Corrales D, Hsu C-H, Aravind L, He C, and Shi Y (2015). DNA Methylation on N6-Adenine in C. elegans. Cell 161, 868–878. [PubMed: 25936839]

Haberle V, Forrest ARR, Hayashizaki Y, Carninci P, and Lenhard B (2015). CAGEr: precise TSS data retrieval and high-resolution promoterome mining for integrative analyses. Nucleic Acids Res 43, e51–e51. [PubMed: 25653163]

Hattman S, Kenny C, Berger L, and Pratt K (1978). Comparative study of DNA methylation in three unicellular eucaryotes. J. Bacteriol 135, 1156–1157. [PubMed: 99431]

Horton JR, Liebert K, Bekes M, Jeltsch A, and Cheng X (2006). Structure and Substrate Recognition of the Escherichia coli DNA Adenine Methyltransferase. J. Mol. Biol 358, 559–570. [PubMed: 16524590]

Huang Y, Niu B, Gao Y, Fu L, and Li W (2010). CD-HIT Suite: a web server for clustering and comparing biological sequences. Bioinformatics 26, 680–682. [PubMed: 20053844]

Huang J, Dong X, Gong Z, Qin L-Y, Yang S, Zhu Y-L, Wang X, Zhang D, Zou T, Yin P, et al. (2018). Solution structure of the RNA recognition domain of METTL3-METTL14 N6-methyladenosine methyltransferase. Protein Cell. 1–13. [PubMed: 29139027]

Huff JT, and Zilberman D (2014). Dnmt1-independent CG methylation contributes to nucleosome positioning in diverse eukaryotes. Cell 156, 1286–1297. [PubMed: 24630728]

Ito T, Bulger M, Pazin MJ, Kobayashi R, and Kadonaga JT (1997). ACF, an ISWI-containing and ATP-utilizing chromatin assembly and remodeling factor. Cell 90, 145–155. [PubMed: 9230310]

Iyer LM, Zhang D, and Aravind L (2016). Adenine methylation in eukaryotes: Apprehending the complex evolutionary history and functional potential of an epigenetic modification. Bioessays 38, 27–40. [PubMed: 26660621]

Karrer KM, and VanNuland TA (1999). Nucleosome positioning is independent of histone H1 *in vivo*. J. Biol. Chem 274, 33020–33024. [PubMed: 10551870]

Katoh K, Rozewicki J, and Yamada KD (2017). MAFFT online service: multiple sequence alignment, interactive sequence choice and visualization. Brief. Bioinform

Kharchenko PV, Tolstorukov MY, and Park PJ (2008). Design and analysis of ChIP-seq experiments for DNA-binding proteins. Nat. Biotechnol 26, 1351–1359. [PubMed: 19029915]

Khurana JS, Wang X, Chen X, Perlman DH, and Landweber LF (2014). Transcription-Independent Functions of an RNA Polymerase II Subunit, Rpb2, During Genome Rearrangement in the Ciliate, *Oxytricha* trifallax. Genetics 197, 839–849. [PubMed: 24793090]

Khurana JS, Clay DM, Moreira S, Wang X, and Landweber LF (2018). Small RNA-mediated regulation of DNA dosage in the ciliate *Oxytricha*. RNA 24, 18–29. [PubMed: 29079634]

Koziol MJ, Bradshaw CR, Allen GE, Costa ASH, Frezza C, and Gurdon JB (2015). Identification of methylated deoxyadenosines in vertebrates reveals diversity in DNA modifications. Nat. Struct. Mol. Biol 23, 24–30. [PubMed: 26689968]

Kuraku S, Zmasek CM, Nishimura O, and Katoh K (2013). aLeaves facilitates on-demand exploration of metazoan gene family trees on MAFFT sequence alignment server with enhanced interactivity. Nucleic Acids Res 41, W22–8. [PubMed: 23677614]

Lai WKM, and Pugh BF (2017). Understanding nucleosome dynamics and their links to gene expression and DNA replication. Nat. Rev. Mol. Cell Biol 18, 548–562. [PubMed: 28537572]

Langmead B, and Salzberg SL (2012). Fast gapped-read alignment with Bowtie 2. Nat. Methods 9, 357–359. [PubMed: 22388286]

Laughlin TJ, Henry JM, Phares EF, Long MV, and Olins DE (1983). Methods for the Large-Scale Cultivation of an *Oxytricha* (Ciliophora: Hypotrichida). J. Protozool 30, 63–64.

Lauth MR, Spear BB, Heumann J, and Prescott DM (1976). DNA of ciliated protozoa: DNA sequence diminution during macronuclear development of *Oxytricha*. Cell 7, 67–74. [PubMed: 820431]

Lawn RM, Heumann JM, Herrick G, and Prescott DM (1978). The gene-size DNA molecules in *Oxytricha*. Cold Spring Harb. Symp. Quant. Biol 42 Pt 1, 483–492. [PubMed: 98283]

Liang Z, Shen L, Cui X, Bao S, Geng Y, Yu G, Liang F, Xie S, Lu T, Gu X, et al. (2018). DNA N 6 - Adenine Methylation in Arabidopsis thaliana. Dev. Cell 45, 406–416.e3. [PubMed: 29656930]

Lieleg C, Ketterer P, Nuebler J, Ludwigsen J, Gerland U, Dietz H, Mueller-Planitz F, and Korber P (2015). Nucleosome spacing generated by ISWI and CHD1 remodelers is constant regardless of nucleosome density. Mol. Cell. Biol 35, 1588–1605. [PubMed: 25733687]

Liu J, Yue Y, Han D, Wang X, Fu Y, Zhang L, Jia G, Yu M, Lu Z, Deng X, et al. (2014). A METTL3-METTL14 complex mediates mammalian nuclear RNA N6-adenosine methylation. Nat. Chem. Biol 10, 93–95. [PubMed: 24316715]

Liu J, Zhu Y, Luo G-Z, Wang X, Yue Y, Wang X, Zong X, Chen K, Yin H, Fu Y, et al. (2016). Abundant DNA 6mA methylation during early embryogenesis of zebrafish and pig. Nat. Commun 7, 13052. [PubMed: 27713410]

Liu Y, Taverna SD, Muratore TL, Shabanowitz J, Hunt DF, and Allis CD (2007). RNAi-dependent H3K27 methylation is required for heterochromatin formation and DNA elimination in *Tetrahymena*. Genes Dev 21, 1530–1545. [PubMed: 17575054]

Livak KJ, and Schmittgen TD (2001). Analysis of relative gene expression data using real-time quantitative PCR and the 2(-Delta Delta C(T)) Method. Methods 25, 402–408. [PubMed: 11846609]

Luger K, Rechsteiner TJ, and Richmond TJ (1999). Preparation of nucleosome core particle from recombinant histones. Methods Enzymol 304, 3–19. [PubMed: 10372352]

Luo G-Z, Blanco MA, Greer EL, He C, and Shi Y (2015). DNA N6-methyladenine: a new epigenetic mark in eukaryotes? Nat. Rev. Mol. Cell Biol 16, 705–710. [PubMed: 26507168]

Luo G-Z, Hao Z, Luo L, Shen M, Sparvoli D, Zheng Y, Zhang Z, Weng X, Chen K, Cui Q, et al. (2018). N6-methyldeoxyadenosine directs nucleosome positioning in *Tetrahymena* DNA. Genome Biol 19, 200. [PubMed: 30454035]

Mavrich TN, Ioshikhes IP, Venters BJ, Jiang C, Tomsho LP, Qi J, Schuster SC, Albert I, and Pugh BF (2008). A barrier nucleosome model for statistical positioning of nucleosomes throughout the yeast genome. Genome Res 18, 1073–1083. [PubMed: 18550805]

Miao W, Xiong J, Bowen J, Wang W, Liu Y, Braguinets O, Grigull J, Pearlman RE, Orias E, and Gorovsky MA (2009). Microarray analyses of gene expression during the *Tetrahymena* thermophila life cycle. PLoS One 4, e4429. [PubMed: 19204800]

Miller MA, Pfeiffer W, and Schwartz T (2010). Creating the CIPRES Science Gateway for Inference of Large Phylogenetic Trees.

Mondo SJ, Dannebaum RO, Kuo RC, Louie KB, Bewick AJ, LaButti K, Haridas S, Kuo A, Salamov A, Ahrendt SR, et al. (2017). Widespread adenine N6-methylation of active genes in fungi. Nat. Genet 49, 964–968. [PubMed: 28481340]

Mortazavi A, Williams BBA, McCue K, Schaeffer L, et al. (2008). Mapping and quantifying mammalian transcriptomes by RNA-Seq. Nat. Methods 5, 621–628. [PubMed: 18516045]

MQller MM, Fierz B, Bittova L, Liszczak G, and Muir TW (2016). A two-state activation mechanism controls the histone methyltransferase Suv39h1. Nat. Chem. Biol 12, 188–193. [PubMed: 26807716]

Murray IA, Morgan RD, Luyten Y, Fomenkov A, Corrêa IR, Dai N, Allaw MB, Zhang X, Cheng X, and Roberts RJ (2018). The non-specific adenine DNA methyltransferase M.EcoGII. Nucleic Acids Res 46, 840–848. [PubMed: 29228259]

Nesvizhskii AI, Keller A, Kolker E, and Aebersold R (2003). A statistical model for identifying proteins by tandem mass spectrometry. Anal. Chem 75, 4646–4658. [PubMed: 14632076]

Nowacki M, Vijayan V, Zhou Y, Schotanus K, Doak TG, and Landweber LF (2008). RNA-mediated epigenetic programming of a genome-rearrangement pathway. Nature 451, 153–158. [PubMed: 18046331]

Pendleton KE, Chen B, Liu K, Hunter OV, Xie Y, Tu BP, and Conrad NK (2017). The U6 snRNA m6A Methyltransferase METTL16 Regulates SAM Synthetase Intron Retention. Cell 169, 824–835.e14. [PubMed: 28525753]

Pratt K, and Hattman S (1981). Deoxyribonucleic acid methylation and chromatin organization in *Tetrahymena* thermophila. Mol. Cell. Biol 1, 600–608. [PubMed: 9279374]

Prescott DM (1994). The DNA of ciliated protozoa. Microbiol. Rev 58, 233–267. [PubMed: 8078435]

Rappsilber J, Mann M, and Ishihama Y (2007). Protocol for micro-purification, enrichment, pre-fractionation and storage of peptides for proteomics using StageTips. Nat. Protoc 2, 1896–1906. [PubMed: 17703201]

Rae PM, and Spear BB (1978). Macronuclear DNA of the hypotrichous ciliate *Oxytricha* fallax. Proc. Natl. Acad. Sci. U. S. A 75, 4992–4996. [PubMed: 105360]

Schäffer AA, Aravind L, Madden TL, Shavirin S, Spouge JL, Wolf YI, Koonin EV, and Altschul SF (2001). Improving the accuracy of PSI-BLAST protein database searches with composition-based statistics and other refinements. Nucleic Acids Res 29, 2994–3005. [PubMed: 11452024]

Schiffers S, Ebert C, Rahimoff R, Kosmatchev O, Steinbacher J, Bohne A-V, Spada F, Michalakis S, Nickelsen J, Müller M, et al. (2017). Quantitative LC-MS Provides No Evidence for m6 dA or m4 dC in the Genome of Mouse Embryonic Stem Cells and Tissues. Angew. Chem. Int. Ed. Engl 56, 11268–11271. [PubMed: 28371147]

Śledź P, and Jinek M (2016). Structural insights into the molecular mechanism of the m(6)A writer complex. Elife 5.

Strahl BD, Ohba R, Cook RG, and Allis CD (1999). Methylation of histone H3 at lysine 4 is highly conserved and correlates with transcriptionally active nuclei in *Tetrahymena*. Proc. Natl. Acad. Sci. U. S. A 96, 14967–14972. [PubMed: 10611321]

Struhl K, and Segal E (2013). Determinants of nucleosome positioning. Nat. Struct. Mol. Biol 20, 267–273. [PubMed: 23463311]

Swart EC, Bracht JR, Magrini V, Minx P, Chen X, Zhou Y, Khurana JS, Goldman AD, Nowacki M, Schotanus K, et al. (2013). The *Oxytricha* trifallax Macronuclear Genome: A Complex Eukaryotic Genome with 16,000 Tiny Chromosomes. PLoS Biol 11, e1001473. [PubMed: 23382650]

Taverna SD, Coyne RS, and Allis CD (2002). Methylation of histone h3 at lysine 9 targets programmed DNA elimination in tetrahymena. Cell 110, 701–711. [PubMed: 12297044]

Wada RK, and Spear BB (1980). Nucleosomal organization of macronuclear chromatin in *Oxytricha* fallax. Cell Differ 9, 261–268.

Wang P, Doxtader KA, and Nam Y (2016a). Structural Basis for Cooperative Function of Mettl3 and Mettl14 Methyltransferases. Mol. Cell 63, 306–317. [PubMed: 27373337]

Wang X, Feng J, Xue Y, Guan Z, Zhang D, Liu Z, Gong Z, Wang Q, Huang J, Tang C, et al. (2016b). Structural basis of N6-adenosine methylation by the METTL3–METTL14 complex. Nature 534, 575–578. [PubMed: 27281194]

Wang Y, Chen X, Sheng Y, Liu Y, and Gao S (2017). N6-adenine DNA methylation is associated with the linker DNA of H2A.Z-containing well-positioned nucleosomes in Pol II-transcribed genes in *Tetrahymena*. Nucleic Acids Res 45, 11594–11606. [PubMed: 29036602]

Warda AS, Kretschmer J, Hackert P, Lenz C, Urlaub H, Höbartner C, Sloan KE, and Bohnsack MT (2017). Human METTL16 is a N^6-methyladenosine (m^6A) methyltransferase that targets pre-mRNAs and various non-coding RNAs. EMBO Rep 18, 2004–2014. [PubMed: 29051200]

Wei Y, Mizzen CA, Cook RG, Gorovsky MA, and Allis CD (1998). Phosphorylation of histone H3 at serine 10 is correlated with chromosome condensation during mitosis and meiosis in *Tetrahymena*. Proc. Natl. Acad. Sci. U. S. A 95, 7480–7484. [PubMed: 9636175]

Wu TP, Wang T, Seetin MG, Lai Y, Zhu S, Lin K, Liu Y, Byrum SD, Mackintosh SG, Zhong M, et al. (2016). DNA methylation on N6-adenine in mammalian embryonic stem cells. Nature 532, 329–333. [PubMed: 27027282]

Xiao R, and Moore DD (2011). DamIP: Using Mutant DNA Adenine Methyltransferase to Study DNA-Protein Interactions In Vivo In Current Protocols in Molecular Biology, (NJ, USA: John Wiley & Sons, Inc.), p. Unit21.21.

Xiao C-L, Zhu S, He M, Chen D, Zhang Q, Chen Y, Yu G, Liu J, Xie S-Q, Luo F, et al. (2018). N6-Methyladenine DNA Modification in the Human Genome. Mol. Cell 71, 306–318.e7. [PubMed: 30017583]

Xiong J, Lu X, Lu Y, Zeng H, Yuan D, Feng L, Chang Y, Josephine B, Gorovsky M, Fu C, et al. (2011). Tetrahymena Gene Expression Database (TGED): A resource of microarray data and co-expression analyses for *Tetrahymena*. Sci. China Life Sci 54, 65–67. [PubMed: 21253873]

Xiong J, Lu X, Zhou Z, Chang Y, Yuan D, Tian M, Zhou Z, Wang L, Fu C, Orias E, et al. (2012). Transcriptome analysis of the model protozoan, Tetrahymena thermophila, using Deep RNA sequencing. PLoS One 7, e30630. [PubMed: 22347391]

Yao B, Cheng Y, Wang Z, Li Y, Chen L, Huang L, Zhang W, Chen D, Wu H, Tang B, et al. (2017). DNA N6-methyladenine is dynamically regulated in the mouse brain following environmental stress. Nat. Commun 8, 1122. [PubMed: 29066820]

Yao B, Li Y, Wang Z, Chen L, Poidevin M, Zhang C, Lin L, Wang F, Bao H, Jiao B, et al. (2018). Active N 6 -Methyladenine Demethylation by DMAD Regulates Gene Expression by Coordinating with Polycomb Protein in Neurons. Mol. Cell

Yerlici VT, and Landweber LF (2014). Programmed Genome Rearrangements in the Ciliate *Oxytricha*. Microbiol. Spectr 2.

Zhang Z, and Pugh BF (2011). High-resolution genome-wide mapping of the primary structure of chromatin. Cell 144, 175–186. [PubMed: 21241889]

Zhang G, Huang H, Liu D, Cheng Y, Liu X, Zhang W, Yin R, Zhang D, Zhang P, Liu J, et al. (2015). N6-Methyladenine DNA Modification in Drosophila. Cell 161, 893–906. [PubMed: 25936838]

Zhou C, Wang C, Liu H, Zhou Q, Liu Q, Guo Y, Peng T, Song J, Zhang J, Chen L, et al. (2018). Identification and analysis of adenine N6-methylation sites in the rice genome. Nat. Plants 4, 554–563. [PubMed: 30061746]

Highlights

- The ciliate methyltransferase MTA1c mediates DNA N6-adenine methylation (6mA)
- 6mA directly disfavors nucleosome occupancy *in vitro*
- Synthesis of complete, epigenetically defined *Oxytricha* chromosomes

Use of designer eukaryotic chromosomes reveals a role for adenine methylation in nucleosome positioning.

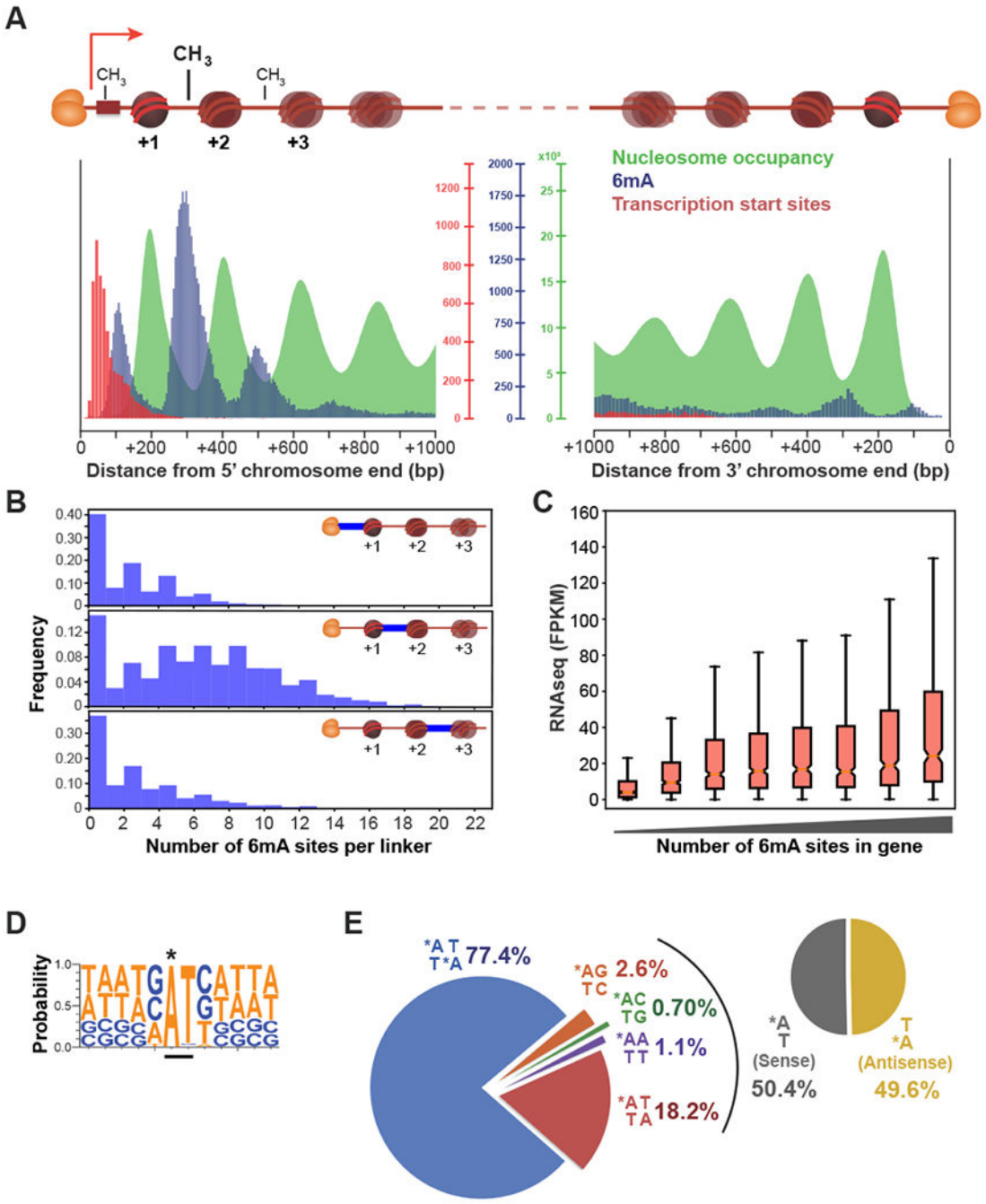

Figure 1. Epigenomic profiles of *Oxytricha* chromosomes

(A) Meta-chromosome plots of chromatin organization at *Oxytricha* macronuclear chromosome ends. Heterodimeric telomere end-binding protein complexes (orange ovals) protect each end *in vivo*. Horizontal red bar: promoter. The 5' chromosome end is proximal to TSSs. "Nucleosome occupancy": normalized MNase-seq coverage; "6mA": total 6mA number; "Transcription start sites": total number of called TSSs.

(B) Histograms of the total number of 6mA marks within each linker in *Oxytricha* chromosomes. Distinct linkers are depicted as horizontal blue lines.

(C) poly(A)-enriched RNAseq levels positively correlate with 6mA. Genes are sorted according to the total number of 6mA marks 0-800 bp downstream of the TSS. FPKM = Fragments per Kilobase of transcript per Million mapped RNAseq reads. Notch in the boxplot denotes median, ends of boxplot denote first and third quartiles, upper whisker denotes third quantile + 1.5 × interquartile range (IQR), and lower whisker denotes data quartile 1 – 1.5 × IQR.

(D) Composite analysis of 65,107 methylation sites reveals that 6mA (marked with *) occurs within an 5'-ApT-3' dinucleotide motif.

(E) Distribution of various 6mA dinucleotide motifs across the genome. Asterisk: 6mA.

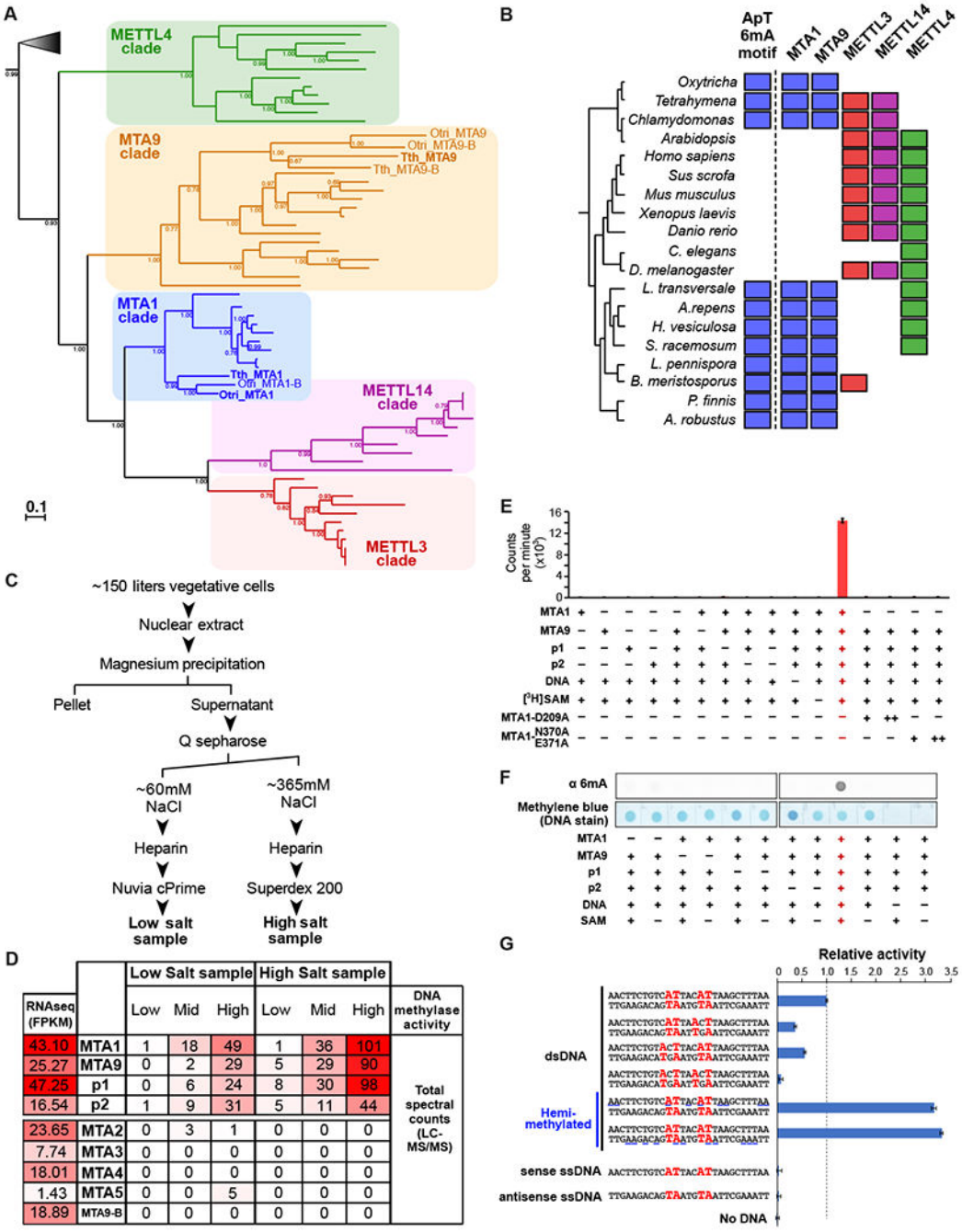

Figure 2. Purification and characterization of the ciliate 6mA methyltransferase

(A) Phylogenetic analysis of MT-A70 proteins. Bold MTA1 and MTA9 genes are experimentally characterized in this study. Paralogs of MTA1 and MTA9 are labeled as "-B". Posterior probabilities > 0.65 are shown. Gray triangle represents outgroup of bacterial sequences. The complete phylogenetic tree is shown in Figure S2G. Gene names are in Table S2. Tth: *Tetrahymena thermophila*; Otri: *Oxytricha trifallax*.

(B) Phylogenetic distribution of the occurrence of ApT 6mA motifs and MT-A70 protein families. Filled square denotes its presence in a taxon. The basal yeast clade is comprised of

L. transversale, A.repens, H. vesiculosa, S. racemosum, L. pennispora, B. meristosporus, P. finnis, and *A. robustus*.

(C) Experimental scheme depicting the partial purification of DNA methyltransferase activity from *Tetrahymena* nuclear extracts.

(D) Gene expression and protein abundance of candidate genes in partially purified *Tetrahymena* nuclear extracts. UniProt IDs are listed in Table S2. RNAseq data are from (Xiong et al., 2012). FPKM = Fragments per Kilobase of transcript per Million mapped RNAseq reads. “Low”, “Mid”, and “High” DNA methylase activity correspond to fractions eluting from the Nuvia cPrime and Superdex 200 columns in panel C. “Total spectrum counts”: total number of LC-MS/MS fragmentation spectra that match peptides from a target protein.

(E) DNA methyltransferase assay using [^{3}H]SAM. Vertical axis represents scintillation counts. Error bars represent s.e.m. (n = 3).

(F) Dot blot assay using cold SAM.

(G) DNA methyltransferase assay performed on different nucleic acid substrates in the presence of MTA1, MTA9, p1, and p2. Sense ssDNA are 5’→3’; antisense are 3’→5’. ApT dinucleotides are labeled in bold red. Horizontal blue lines in hemimethylated dsDNA substrates denote possible locations where 6mA may be installed by *EcoGII* (prior to this assay). “Relative activity” denotes scintillation counts normalized against the unmethylated 27bp dsDNA substrate with two ApT motifs (top-most dsDNA substrate). An enlarged bar plot of relative activity on 27bp unmethylated dsDNA substrates is included in Figure S3K. Error bars represent s.e.m. (n = 3).

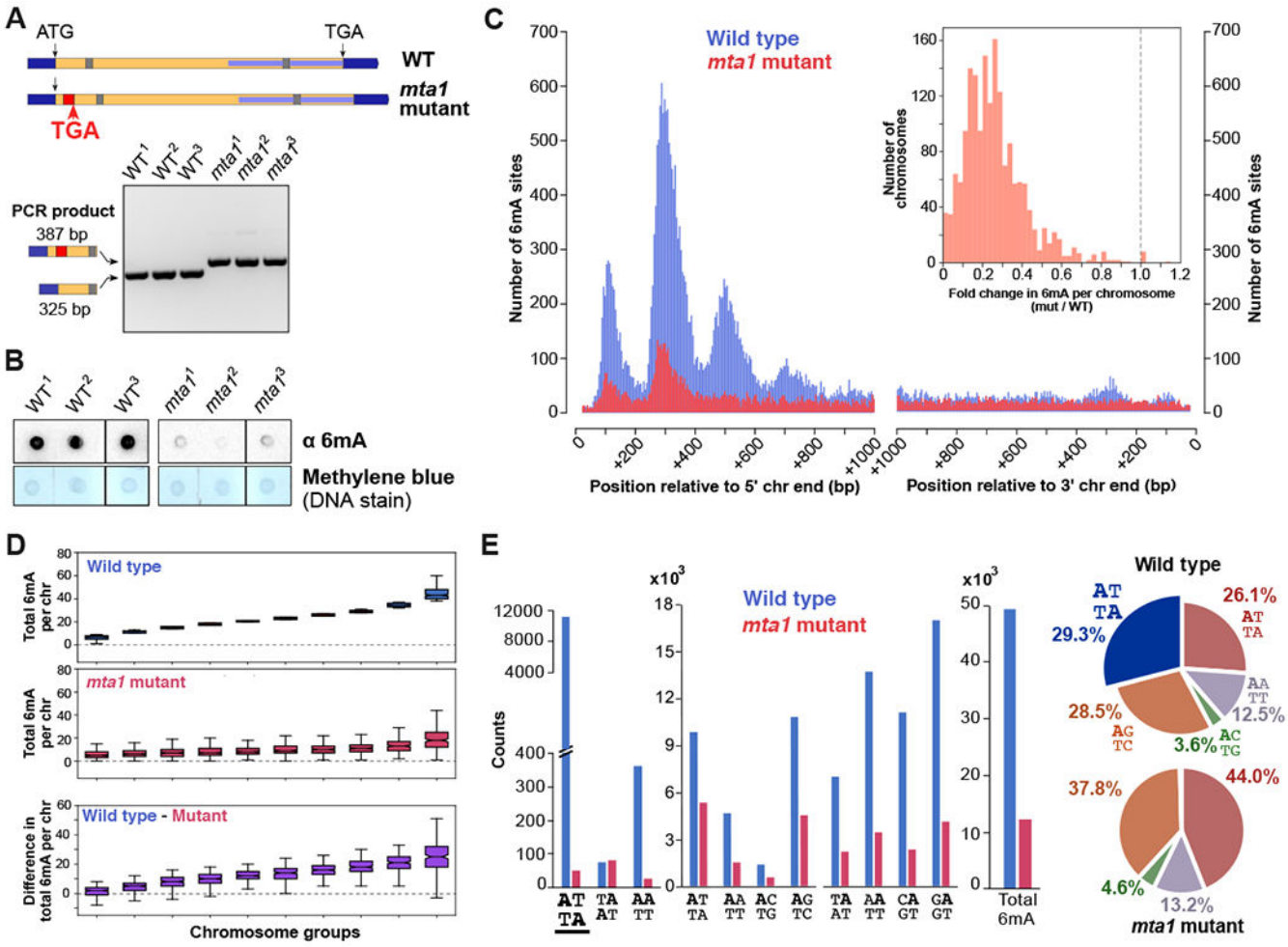

Figure 3. Genome-wide loss of 6mA in *mta1* mutants

(A) Schematic depicting the disruption of *Oxytricha* MTA1 open reading frame. Flanking dark blue bars: 5' and 3' UTR; yellow = open reading frame; red = retention of 62 bp ectopic DNA segment; grey bar = intron; internal light blue bar = annotated MT-A70 domain; "ATG" = start codon; "TGA" = stop codon. Agarose gel analysis shows PCR confirmation of ectopic DNA retention.

(B) Dot blot analysis of RNase-treated genomic DNA.

(C) Histogram of 6mA counts near 5' and 3' *Oxytricha* chromosome ends. Inset depicts histogram of fold change in total 6mA in each chromosome, between mutant and wild type cell lines.

(D) Chromosomes are sorted into 10 groups according to total 6mA in wild type cells (blue boxplots). For each group, the total 6mA per chromosome in mutants, and the difference in total 6mA per chromosome is plotted below. Boxplot features are as described in Figure 1C.

(E) Motif distribution in wild type and *mta1* mutants. Loss of ApT dimethylated motif is underlined.

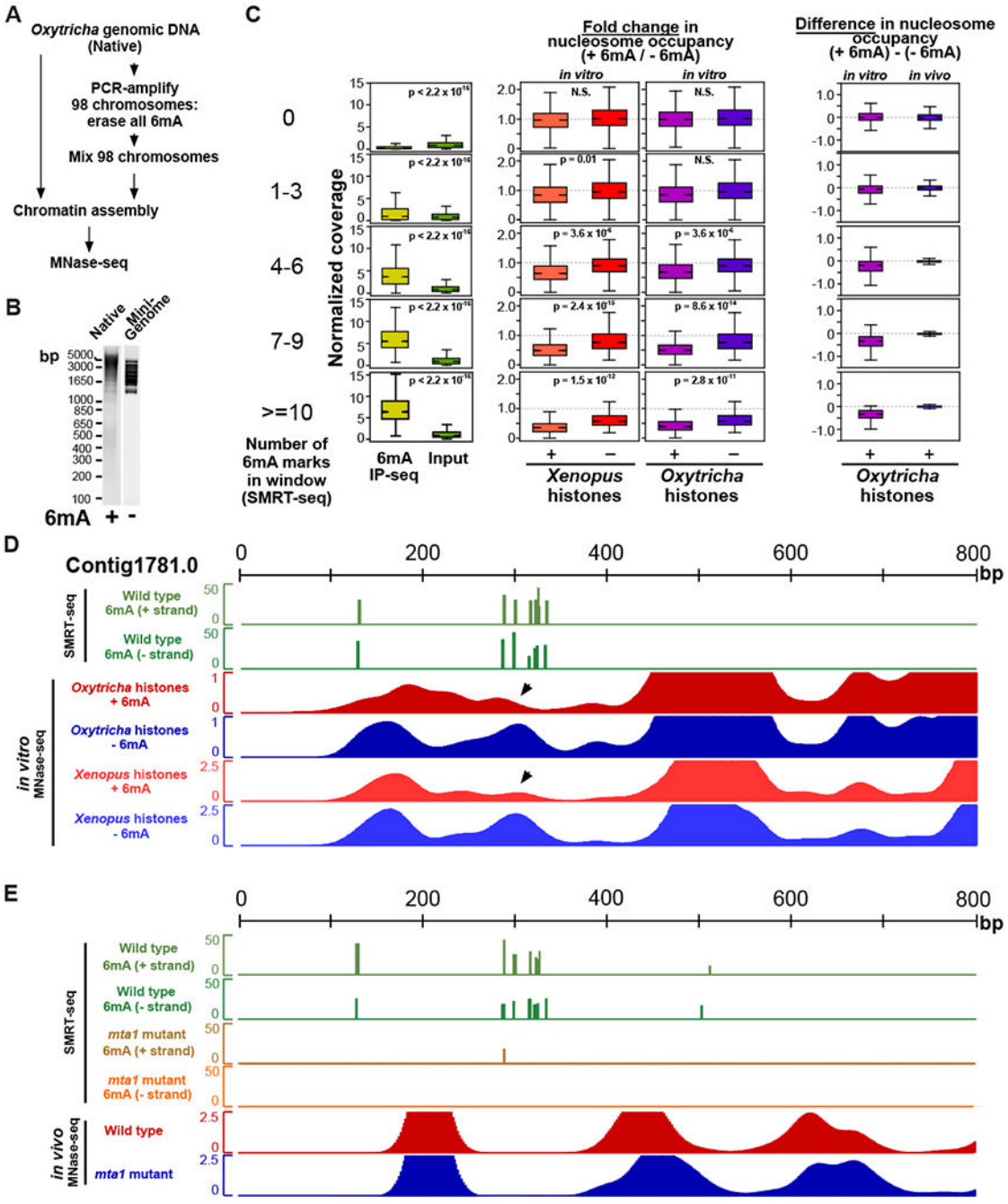

Figure 4. Effects of 6mA on nucleosome organization *in vitro* and *in vivo*

(A) Experimental workflow for the generation of mini-genome DNA.

(B) Agarose gel analysis of *Oxytricha* gDNA ('Native') and mini-genome DNA before chromatin assembly.

(C) Methylated regions exhibit lower nucleosome occupancy *in vitro* but not *in vivo*. Overlapping 51bp windows were analyzed across 98 chromosomes. For each window, the change in nucleosome occupancy in the absence versus presence of 6mA was calculated.

Boxplot features are as described in Figure 1C. *P*-values were calculated using a two-sample unequal variance t-test. "N.S": non-significant, with $p > 0.05$.

(D) Reduction in nucleosome occupancy at methylated loci *in vitro* (black arrowheads). For *in vitro* MNase-seq, "+ 6mA" refers to chromatin assembled on *Oxytricha* gDNA, while "−6mA" denotes chromatin assembled on mini-genome DNA. Vertical axis for SMRT-seq data denotes confidence score [−10 log(p-value)] of detection of 6mA, while that for *in vitro* MNase-seq data denotes nucleosome occupancy.

(E) No change in nucleosome occupancy in linker regions despite loss of 6mA in *mta1* mutants. Vertical axes are the same as panel (D).

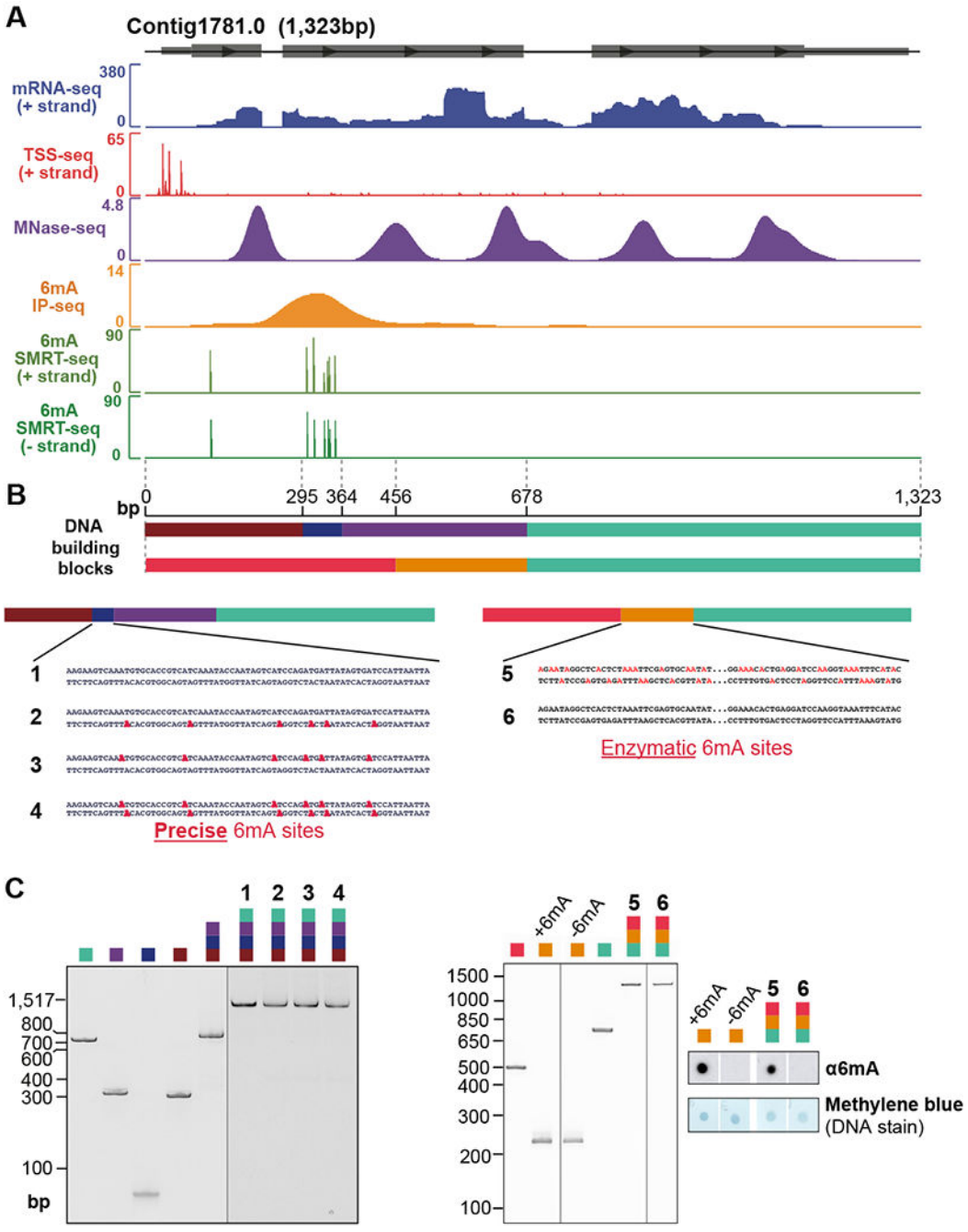

Figure 5. Modular synthesis of full-length *Oxytricha* chromosomes

(A) Features of the chromosome selected for synthesis. Grey boxes represent exons. All data tracks represent normalized coverage except for SMRT-seq, which represents the confidence score [−10 log(p-value)] of detection of each methylated base.

(B) Schematic of chromosome construction. Different colors denote DNA building blocks ligated to form the full-length chromosome. Precise 6mA sites (bold red) represent cognate 6mA positions revealed by SMRT-seq in native genomic DNA. These are introduced via oligonucleotide synthesis. For chromosome 5, 6mA sites (non-bold red) represent possible

locations ectopically installed by a bacterial 6mA methyltransferase, *EcoGII*. Intervening sequence within chromosomes 5 and 6 is represented as "…"

(C) Native polyacrylamide gel analysis and anti-6mA dot blot analysis of building blocks and purified synthetic chromosomes.

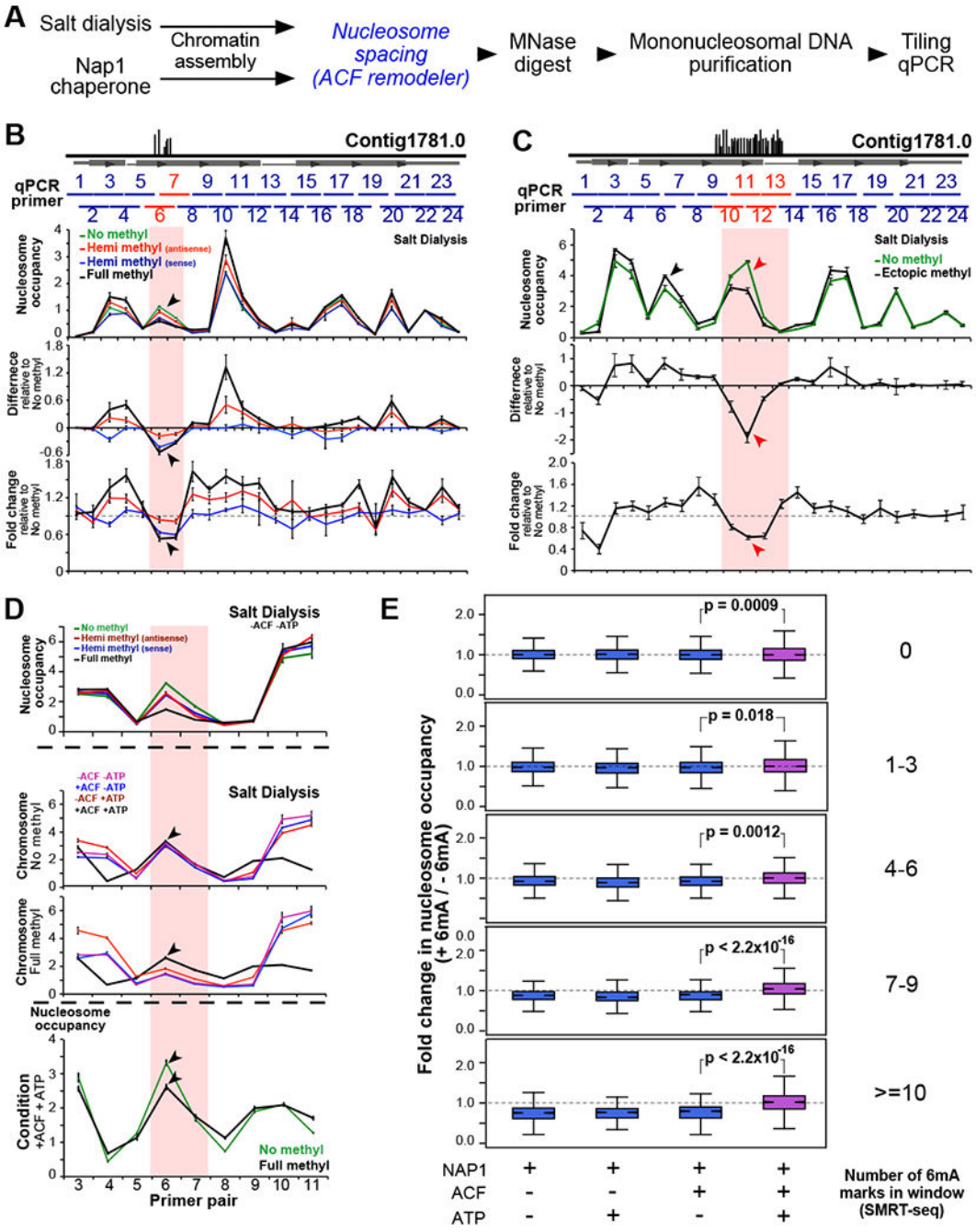

Figure 6. Quantitative modulation of nucleosome occupancy by 6mA

(A) Experimental workflow. Chromatin is assembled using either salt dialysis or the NAP1 histone chaperone. Italicized blue steps are selectively included.

(B) Tiling qPCR analysis of synthetic chromosome with cognate 6mA sites. Horizontal grey box represents annotated gene, and vertical black lines depict native 6mA positions. Horizontal blue bars span ~100bp regions amplified by qPCR. Red horizontal lines represent the region containing 6mA. 'Hemi methyl' chromosomes contain 6mA on the antisense and

sense strands, respectively, while the ‘Full methyl’ chromosome has 6mA on both strands. Black arrowheads: decrease in nucleosome occupancy specifically at the 6mA cluster.
(C) Tiling qPCR analysis of ectopically methylated synthetic chromosome. Vertical black lines illustrate possible 6mA sites installed enzymatically. Red arrowheads: decrease in nucleosome occupancy in the ectopically methylated region. Black arrowheads: position of cognate 6mA sites (not in this construct).
(D) Tiling qPCR analysis of chromatin from panel B that is subsequently incubated with ACF and/or ATP. ACF equalizes nucleosome occupancy between the 6mA cluster and flanking regions in the presence of ATP (black line). Nucleosome occupancy at the methylated region is not restored to the same level as the unmethylated control (black arrowheads).
(E) MNase-seq analysis of chromatin is assembled on native gDNA (“+” 6mA) and mini-genome DNA (“−“ 6mA) using NAP1 +/− ACF and ATP. *P*-values were calculated using a two-sample unequal variance t-test.

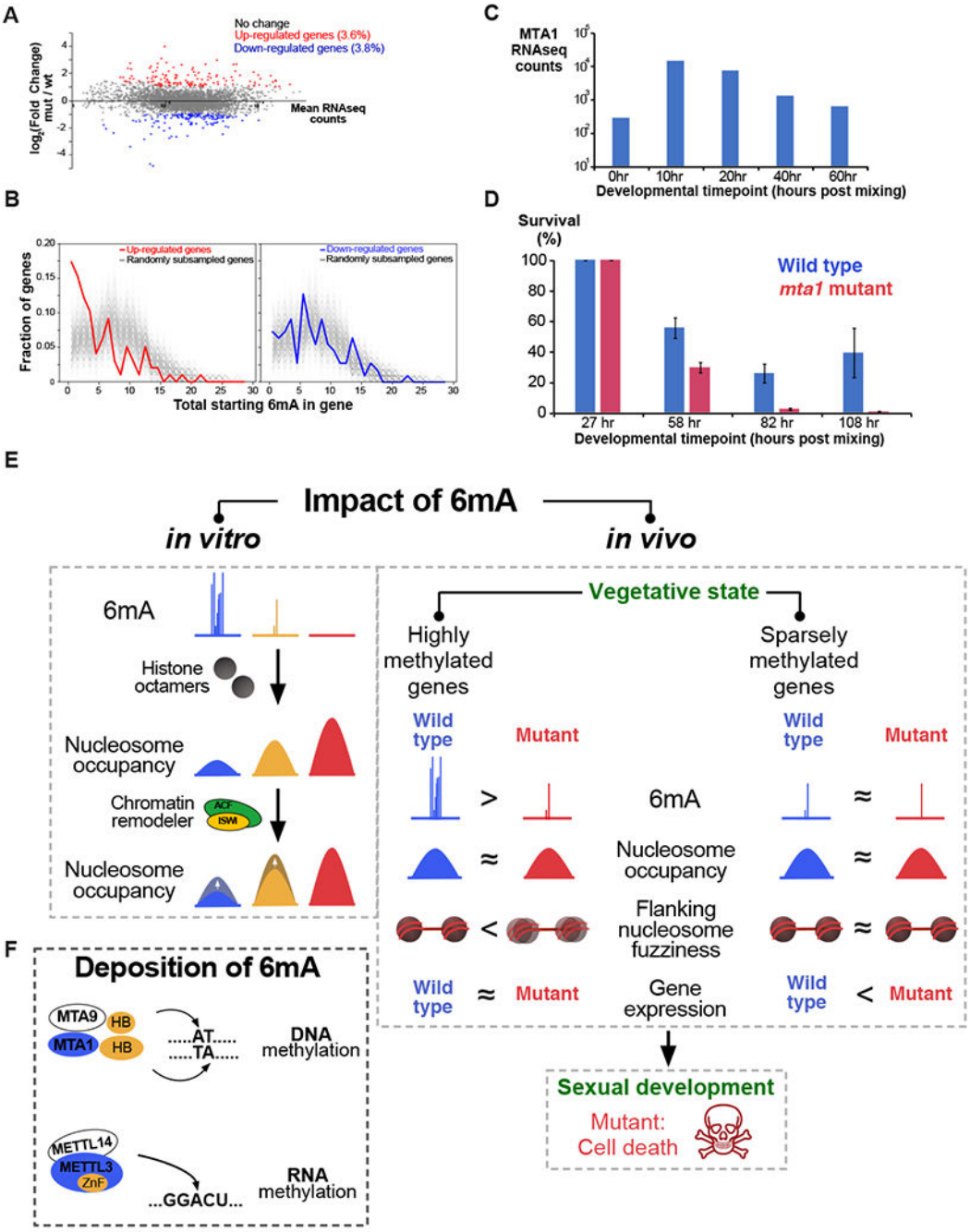

Figure 7. Effects of 6mA on gene expression and cell viability *in vivo*.

(A) Horizontal axis: the mean RNAseq counts across all biological replicates from wild type and *mta1* mutant data for each gene. Vertical axis: $\log_2$(fold change) in gene expression (mutant / wild type).

(B) Upregulated genes tend to be sparsely methylated compared to randomly subsampled genes (grey lines). See Methods for analysis procedure.

(C) RNAseq analysis of MTA1 expression during the sexual cycle of *Oxytricha*. RNAseq timecourse data are from (Swart et al., 2013). The total duration of the sexual cycle is ~60 hr.

(D) Survival analysis of *Oxytricha* cells during the sexual cycle. The total cell number at each timepoint is normalized to 27 hr data to obtain the percentage survival. Error bars represent s.e.m. (n = 4).

(E) Model illustrating the impact of 6mA methylation by MTA1c on nucleosome organization and gene expression.

(F) Comparison of DNA and RNA N6-adenine methyltransferases. Blue denotes catalytic subunit, yellow denotes subunit with predicted DNA or RNA binding domain.